Title

Spinal subpial delivery of AAV9 enables widespread gene silencing and blocks motoneuron degeneration in ALS

Journal

Nature Medicine, 26(1)

ISSN

1078-8956

Authors

Bravo-Hernandez, Mariana
Tadokoro, Takahiro
Navarro, Michael R
et al.

Publication Date

2020

DOI

10.1038/s41591-019-0674-1

Peer reviewed

HHS Public Access

Author manuscript

Nat Med. Author manuscript; available in PMC 2021 June 02.

Published in final edited form as:

Nat Med. 2020 January ; 26(1): 118–130. doi:10.1038/s41591-019-0674-1.

Spinal subpial delivery of AAV9 enables widespread gene silencing and blocks motoneuron degeneration in ALS

Mariana Bravo-Hernandez[1,13], **Takahiro Tadokoro**[1,2,13], **Michael R. Navarro**[1], **Oleksandr Platoshyn**[1], **Yoshiomi Kobayashi**[1], **Silvia Marsala**[1], **Atsushi Miyanohara**[1,3], **Stefan Juhas**[4], **Jana Juhasova**[4], **Helena Skalnikova**[4], **Zoltan Tomori**[5], **Ivo Vanicky**[6], **Hana Studenovska**[7], **Vladimir Proks**[7], **PeiXi Chen**[1], **Noe Govea-Perez**[1,8], **Dara Ditsworth**[8], **Joseph D. Ciacci**[9], **Shang Gao**[10], **Wenlian Zhu**[10], **Eric T. Ahrens**[10], **Shawn P. Driscoll**[11], **Thomas D. Glenn**[11], **Melissa McAlonis-Downes**[8], **Sandrine Da Cruz**[8], **Samuel L. Pfaff**[11], **Brian K. Kaspar**[12], **Don W. Cleveland**[8], **Martin Marsala**[1,6,*]

[1]Neuroregeneration Laboratory, Department of Anesthesiology, University of California San Diego, La Jolla, CA, USA.

[2]Department of Anesthesiology, University of the Ryukyus, Okinawa, Japan.

[3]Vector Core Laboratory, University of California San Diego, La Jolla, CA, USA.

[4]Institute of Animal Physiology and Genetics, AS CR v.v.i., Liběchov, Czech Republic.

[5]Dept. of Biophysics, Institute of Experimental Physics, Slovak Academy of Sciences, Kosice, Slovakia.

[6]Institute of Neurobiology, Slovak Academy of Sciences, Kosice, Slovakia.

[7]Department of Biomaterials and Bioanalogous System, Institute of Macromolecular Chem35istry, Czech Academy of Sciences, Prague, Czech Republic.

[8]Ludwig Institute for Cancer Research and Department of Cellular and Molecular Medicine, University of California San Diego, La Jolla, CA, USA.

[*]**Correspondence and requests for materials** should be addressed to M.M. mmarsala@ucsd.edu.

Author contributions

M.B.-H. and T.T. performed the mouse in vivo part of the study. M.R.N. and P.C. performed immunofluorescence staining, and quantitative and qualitative immunofluorescence image analysis. O.P. performed electrophysiologic recordings. Y.K., S.J., N.G.-P., J.D.C., H. Skalnikova, H. Studenovska, V.P. and J.J. performed the large animal studies. A.M. produced and validated the AAV9 vectors. S.G., W.Z. and E.T.A. performed postmortem MRI analysis. S.P.D., T.D.G. and S.L.P. conducted mRNA-seq analysis. Z.T. and I.V. performed qualitative and quantitative axon analysis. M.M.-D. performed animal breeding and genotyping. B.K.K., D.W.C. and M.M. designed the study and prepared the manuscript. All authors contributed to the final editing and approval of the manuscript. S.M., D.D. and S.D.C. were the project managers.

Competing interests

M. Marsala is the scientific founder of Neurgain Technologies, Inc. and has an equity interest in the company. In addition, he serves as a consultant to Neurgain Technologies, Inc., and receives compensation for these services. The terms of this arrangement have been reviewed and approved by the University of California San Diego in accordance with its policies on conflict of interests. B.K.K. is a Chief Scientific Officer in Avexis Inc. All other authors declare that no competing interests exist.

Reprints and permissions information is available at www.nature.com/reprints.

Extended data is available for this paper at https://doi.org/10.1038/s41591–019-0674–1.

Supplementary information is available for this paper at https://doi.org/10.1038/s41591–019-0674–1.

Peer review information Brett Benedetti and Kate Gao were the primary editors on this article, and managed its editorial process and peer review in collaboration with the rest of the editorial team.

[9]Department of Neurosurgery, University of California San Diego, La Jolla, CA, USA.

[10]Department of Radiology, University of California San Diego, La Jolla, CA, USA.

[11]Gene Expression Laboratory and the Howard Hughes Medical Institute, Salk Institute for Biological Studies, La Jolla, CA, USA.

[12]Avexis Inc., Chicago, IL, USA.

[13]These authors contributed equally: M. Bravo-Hernandez, T. Tadokoro.

Abstract

Gene silencing with virally delivered shRNA represents a promising approach for treatment of inherited neurodegenerative disorders. In the present study we develop a subpial technique, which we show in adult animals successfully delivers adeno-associated virus (AAV) throughout the cervical, thoracic and lumbar spinal cord, as well as brain motor centers. One-time injection at cervical and lumbar levels just before disease onset in mice expressing a familial amyotrophic lateral sclerosis (ALS)-causing mutant *SOD1* produces long-term suppression of motoneuron disease, including near-complete preservation of spinal α-motoneurons and muscle innervation. Treatment after disease onset potently blocks progression of disease and further α-motoneuron degeneration. A single subpial AAV9 injection in adult pigs or non-human primates using a newly designed device produces homogeneous delivery throughout the cervical spinal cord white and gray matter and brain motor centers. Thus, spinal subpial delivery in adult animals is highly effective for AAV-mediated gene delivery throughout the spinal cord and supraspinal motor centers.

The technology for in vivo gene silencing has opened a new field of experimental and clinical gene-based therapies, which can target disease-causing somatic cell mutations. It is expected that, if an effective delivery of the silencing vector (such as AAV9-based silencing vectors) into the target cell population is achieved, it will be associated with a long-lasting therapeutic effect. Genetic disorders affecting the central nervous system, including ALS, represent an important target for employing a gene-silencing approach as a potential treatment. Specifically, silencing the expression of mutations in the cytoplasmic superoxide dismutase (*SOD1*) gene that causes ALS has been extensively studied, and the approach is currently being considered as a primary clinical target1–4. A well-characterized neuropathologic hallmark of *SOD1* gene mutation expression is widespread neuronal degeneration of spinal α-motoneurons and interneurons, descending motor tracts and alteration in glial (microglia, astrocyte and oligodendrocyte) function5–10. These data suggest that an effective silencing-vector-based therapy needs to target multiple cell types within the neuraxis, including descending/ascending spinal axons, α-motoneurons and interneurons, as well as glial cells9,11,12. In addition, as most hereditary forms of ALS are diagnosed in adult patients (including disease from mutations in *SOD1*), a critical requirement for a vector-based therapy to provide clinically relevant treatment is effective delivery of the silencing vector through the neuraxis in adult individuals.

Several molecularly distinct strategies, all aimed at decreasing the synthesis of mutated SOD1 protein, are being tested in preclinical and clinical studies including: (1) micro-RNA,

(2) shRNA and (3) antisense oligonucleotides13–18. Although good penetrability into the central nervous system and spinal cord are seen after intrathecal (IT) or intraventricular (ICV) delivery of antisense oligonucleotides, one of the major limitations in using viral delivery vectors (including AAV) is, however, their requirement for high titers for at least partial penetration into the adult CNS after systemic or ICV/IT delivery. This limits the feasibility, effectiveness and safety of using AAV9-based silencing vectors in *SOD1*-mutation-linked animal models of ALS4,15,16,19.

To address these limitations, we report the use of a new silencing vector-delivery technique that employs a spinal subpial (SP) approach. We demonstrate in adult mice, pigs and non-human primates (NHPs) that SP AAV9 injection produces homogeneous delivery to most or all cell types in the spinal cord and brain motor centers20,21. Single injections at cervical and upper lumbar levels of silencing vector in adult mice expressing an ALS-causing mutation in *SOD1*, applied just before disease onset or symptomatic animals, are shown, respectively, to prevent or block ongoing motor neuron degeneration.

Results

Combined SP cervical and lumbar delivery of AAV9–shRNA–*SOD1* in adult *SOD1*^{G37R} mice leads to long-term preservation of motor function.

We first studied the spread of an AAV9 vector after spinal SP (Fig. 1a–c) or IT injections in wild-type B6 adult mice (n = 12). Animals received two SP injections of AAV9–UBI–ribosomal protein L22 tagged with 3xHA (*Rpl22*-3x*HA*) (10 μl; 1.2 × 1013 genome copies (GC) ml−1) or AAV9–UBI–*GFP* (10 μl; 1.4 × 1013 GC ml−1), one at the C4 and the second at the L1 level, or a single lumbar IT injection of AAV9–UBI–*GFP* (10 μl; 1.4 × 1013 GC ml−1).

Animals were sacrificed 48 h (AAV9–UBI–*Rpl22*-3x*HA*) or 14 d (AAV9–UBI–*GFP*) after injection. Widespread cellular Rpl22 expression (HA (human influenza hemagglutinin) + staining) was seen between cervical and lumbar segments (Fig. 1b; and see Extended Data Fig. 1a–c). Green fluorescent protein (GFP) + neurons were also found throughout the motor cortex, nucleus ruber and reticular formation (Fig. 1c; and see Extended Data Fig. 1d–h), presumably the result of descending motor axon infection.

We next compared the efficacy of AAV9-mediated gene expression in mice injected either subpially or intrathecally with AAV9–UBI–*GFP*. IT injection produced GFP expression limited to a subpopulation of spinal α-motoneurons and primary afferents, with no expression in interneurons and only an occasional GFP + neuron in brain motor centers (see Extended Data Fig. 2a,b). In contrast, with single SP injections at cervical and lumbar levels, GFP was expressed broadly in spinal NeuN (hexaribonucleotide binding protein-3) + neurons and surrounding glia (see Extended Data Fig. 2c) in all spinal segments (see Extended Data Fig. 2e) and brain motor centers (see Extended Data Fig. 2d).

SOD1^{G37R} transgenic mice22–24 start to accumulate misfolded SOD1 protein in gray matter at an approximate age of 150 d (ref. 25; see Supplementary Fig. 1) and display initial gait abnormalities at ~340 d (ref. 23). To evaluate the most potent route of silencing vector

delivery (to be used in long-term efficacy studies), we next compared the level of spinal *SOD1*^{G37R} silencing after lumbar SP versus IT AAV9–shRNA–*SOD1* (10 μl; 2.8 × 1012 GC ml−1) delivery in adult (age ~118 d) *SOD1*^{G37R} mice. At 4 weeks after vector delivery, FISH and quantitative PCR (qPCR) analysis showed ~80% reduction in *SOD1*^{G37R}-encoding messenger RNA in subpially injected animals, with no notable decrease in intrathecally injected mice (see Extended Data Fig. 2f,g).

Based on the superior potency of subpially delivered AAV9–shRNA–*SOD1* in decreasing spinal *SOD1*^{G37R} mRNA, cohorts of *SOD1*^{G37R} mice (both sexes) and their nontransgenic littermates were injected subpially at cervical and lumbar sites with AAV9–shRNA–*SOD1* (10 μl for each site; 2.8 × 1012 GC ml−1) before disease onset or mid-disease (average ages of ~120 d or 348 d, respectively) (Fig. 1d,e). The cohorts comprised seven groups: (1) *SOD1*^{G37R} shamo-perated mice (n = 14; 9 females and 5 males aged ~120 d); (2) *SOD1*^{G37R} mice subpially treated with AAV9–shRNA–*SOD1* (n = 17; 9 females and 8 males aged ~120 d); (3) *SOD1*^{G37R} mice subpially treated with AAV9–shRNA–*SOD1* (n = 4; 2 females and 2 males aged ~348 d); (4) *SOD1*^{G37R} mice subpially treated with an AAV9-empty vector (scrambled) or sham-operated mice (n = 4; 3 females and 1 male aged ~348 d); (5) *SOD1*^{G37R} nontreated mice (n = 4; 3 females and 1 male); (6) *SOD1*^{G37R} nontreated mice (n = 3; 1 female and 2 males perfused at age 348 ± 2 d); and (7) wild-type nontransgenic mice (n = 13; 5 females and 8 males). Animals were tested for: (1) disease onset (defined by a 20% decrease in grip strength and open-field motor performance); (2) disease end-stage (defined by the loss of righting reflex); (3) forelimb and hindlimb grip strength; and (4) open-field motor performance.

Remarkably, *SOD1*^{G37R} animals treated before disease onset by SP delivery (at age 120 d) of AAV9–shRNA–*SOD1* never developed motoneuron disease (when followed to average age of 462 d), including absence of loss of grip strength, righting reflex and open-field performance (Fig. 1f–l; see Supplementary Video 1). In untreated and sham-operated animals, disease onset initiated at age ~306 d (Fig. 1f,g), with a loss of forelimb and hindlimb grip strength (Fig. 1i,j), reached the end-stage at 389 and 395 d, respectively (Fig. 1h). Although open-field motor performance declined by 60% by ~390 d in sham-operated *SOD1*^{G37R} animals, no notable decrease was measured in AAV9–shRNA–*SOD1*-treated *SOD1*^{G37R} animals aged up to ~470 d (Fig. 1k,l).

Despite the absence of motoneuron disease in treated *SOD1*^{G37R} animals, mice were sacrificed at age ~470 d based on (1) the loss of two animals during grip strength testing from apparent cardiac arrest and (2) an additional two animals that died overnight without disease-related neurologic symptoms. Recognizing that hemodynamic changes caused by autonomic dysreflexia have been reported in symptomatic ALS patients26–28, potential contributions of autonomic misbalance in sudden death in *SOD1*^{G37R} mice were examined after electrical c-fiber stimulation of the hind paw or direct electrical stimulation of the vagal nerve in *SOD1*^{G37R} mice29,30, with changes in heart rate (HR) used as a functional readout. Electrical paw stimulation in wild-type (nontransgenic) and presymptomatic *SOD1*^{G37R} animals led to a transient increase in HR. In contrast, the same stimulation performed in symptomatic *SOD1*^{G37R} mice triggered a decrease in HR (see Supplementary Fig. 2a,b). Direct vagal nerve stimulation in wild-type animals led to a transient, 10–15% decrease in

HR during continuous 5-Hz or 10-Hz stimulation. In presymptomatic *SOD1*^{G37R} mice more pronounced bradycardia (up to 50% decrease in HR) was measured at a 10-Hz stimulation frequency (see Supplementary Fig. 2c,d). In symptomatic animals, a second train of vagal nerve stimulation at 10 Hz led to a profound decrease in the HR, which was then followed by cardiac arrest (see Supplementary Fig. 2c). Qualitative and quantitative histologic analysis of parabrachial sympathetic ganglia showed ~40% reduction in a number of tyrosine hydroxylase (TH+)-expressing neurons. Axon survival in the vagus nerve was reduced ~45% compared with wild-type (nontransgenic) animals (see Supplementary Fig. 2e–h). These data demonstrate that exacerbated, parasympathetic systemmediated responses evoked by stressful conditions may result in a critical decrease in HR and cardiac arrest in *SOD1*^{G37R} mice. Similar degeneration of sympathetic ganglia, and a prevalent vagally mediated effect that can predispose to life-threating arrhythmias, have been described in late-stage ALS patients. Pharmacologic treatment is effective in controlling these symptoms in most of these patients26–28,31,32.

SP AAV9 delivery of shRNA to *SOD1* in *SOD1*^{G37R} mice preserves myogenic motor–evoked potentials and suppresses peripheral denervation-induced MF.

We assessed the functional integrity of descending motor pathways to the neuromuscular junction (NMJ) (in the gastrocnemius muscle (GCM)) and the degree of hindlimb muscle denervation (defined by the presence of muscle fibrillation (MF) in recorded GCM electromyography (EMG) signal) in *SOD1*^{G37R} mice injected before disease onset (at ~120 d) with AAV9–shRNA–*SOD1*. Motor evoked potentials (MEPs) and MFs were recorded at age ~477 d (Fig. 2a,b). In wild-type mice, high-amplitude MEPs were recorded. No MEP responses were recorded in any sham-operated *SOD1*^{G37R} animals at the age of sacrifice (~390 d). In contrast, all AAV9–shRNA–*SOD1*-treated *SOD1*^{G37R} animals showed persistent MEPs measured at an average age of ~477 d (Fig. 2c,d). Recording of MFs showed their absence in age-matched, wild-type, nontransgenic animals. All sham-operated *SOD1*^{G37R} animals displayed high-amplitude MFs. In shRNA–*SOD1*-treated *SOD1*^{G37R} animals, no MFs were measured (Fig. 2e,f).

Although analysis of thoracic spinal cord sections from untreated *SOD1*^{G37R} animals showed a high degree of white matter disintegration, axon and neuropil protection, similar to that in wild-type nontransgenic mice, was seen in AAV9–shRNA–*SOD1*-treated *SOD1*^{G37R} animals (Fig. 2g,h; and see Supplementary Fig. 3a–c). Similarly, although myelinated axon degeneration in the sciatic nerve was present in sham-operated *SOD1*^{G37R} mice, these axons were preserved in subpially treated *SOD1*^{G37R} animals (Fig. 2i,j; and see Supplementary Fig. 4a–g). Consistent with the near absence of MFs and sciatic nerve motor axon preservation in shRNA–*SOD1*^{G37R}-treated animals, NMJs in GCM remained normal (similar to nontransgenic animals) in AAV–shRNA–*SOD1*-treated animals (see Extended Data Fig. 3a,c, white arrows). In contrast, a denervated NMJ developed in sham-operated animals (see Extended Data Fig. 3b, white arrows).

SP delivery with AAV9 of shRNA to *SOD1* preserves spinal α-motoneurons and interneurons, and suppresses misfolded SOD1 in *SOD1^{G37R}* mice.

Compared with wild-type nontransgenic mice (Fig. 3a), a loss of α-motoneurons at all levels of the spinal cord developed by age ~390 d in sham-operated *SOD1^{G37R}* animals (Fig. 3b, and see Extended Data Fig. 4a). In AAV9–shRNA–*SOD1*-treated *SOD1^{G37R}* animals (Fig. 3c, and see Extended Data Fig. 4b), no detectable differences were seen and the number of normally appearing α-motoneurons was similar to wild-type nontransgenic mice (Fig. 3g, and see Extended Data Fig. 4c). Although interneurons (marked by NeuN staining between laminae III and VII) were decreased in sham-operated *SOD1^{G37R}* animals (Fig. 3d,e, and see Extended Data Fig. 4a,c), AAV9–shRNA–*SOD1*-treated animals maintained NeuN-reactive interneurons similar to wild-type nontransgenic mice (Fig. 3d,f,h and see Extended Data Fig. 4b,c). Misfolded SOD1 protein (detected with the B8H10 antibody), which showed a dense accumulation of SOD1 aggregates throughout the spinal cord of sham-operated *SOD1^{G37R}* animals (Fig. 3b), was potently suppressed in AAV9–shRNA–*SOD1*-treated *SOD1^{G37R}* animals (Fig. 3c,i).

SP AAV9 delivery of shRNA blocks spinal cord atrophy and suppresses spinal inflammatory changes in *SOD1^{G37R}* mice.

Quantitative, volumetric, magnetic resonance imaging (MRI)-based analysis of lumbar spinal segments showed preservation of gray matter volume in AAV9–shRNA–*SOD1*-treated *SOD1^{G37R}* animals compared with wild-type nontransgenic mice, whereas there was a significant decrease in gray matter volume and gray matter/white matter index in sham-operated *SOD1^{G37R}* animals (Fig. 4a,b). Analysis of spinal inflammatory changes (compared with wild-type nontransgenic animals) revealed astrocyte and microglial activation in sham-operated *SOD1^{G37R}* animals (Fig. 4c,d,f,g). This was less pronounced in AAV9–shRNA–*SOD1*-treated *SOD1^{G37R}* animals compared with wild-type nontransgenic mice (Fig. 4e,h; compare Fig. 4c–e and 4f–h; see also Fig. 4i,j).

Mutant *SOD1^{G37R}* mRNAs (detected by FISH) (Fig. 4k–s) and qPCR in spinal parenchyma were prominent throughout the entirety of the spinal cord of *SOD1^{G37R}* mice (Fig. 4l,o,r). In shRNA–*SOD1*-treated *SOD1^{G37R}* animals, a clear loss of *hSOD1* mRNA was seen throughout the spinal cord (Fig. 4m,p,s) with 65–75% reductions (measured by qPCR) in mutant *SOD1* mRNA (Fig. 4t; and see Supplementary Fig. 5a). A corresponding, notable reduction in hSOD1 protein expression was seen (using immunoblotting) in the cervical, thoracic and lumbar spinal cord (Fig. 4u; and see Supplementary Fig. 5b–d and Source Data Fig. 1). There was no effect on mutant SOD1 expression in peripheral organs (for example, liver) (Fig. 4v; and see Supplementary Fig. 5e) and in brain regions (brain stem) that do not project axons into the spinal cord (see Supplementary Fig. 6).

SP AAV9 delivery of shRNA suppresses spinal parenchymal disease-dependent gene expression changes in *SOD1^{G37R}* mice.

Whole-transcriptome mRNA sequencing analysis of lumbar spinal cords revealed 6,884 genes differentially expressed in end-stage *SOD1^{G37R}* animals compared with age-matched, wild-type mice (see Extended Data Fig. 5a,b,e and Supplementary Table 1). Clustering analysis of whole-transcriptome gene expression demonstrated that AAV9–shRNA–*SOD1*-

treated *SOD1*^{G37R} animals clustered with wild-type nontransgenic animals, whereas the untreated and sham-operated *SOD1*^{G37R} animals (analyzed at disease end-stage) clustered separately (see Extended Data Fig. 5c,d). Of the genes that were altered in *SOD1*^{G37R} animals, the vast majority (88%) showed nearnormal expression levels in the shRNA–*SOD1*-treated *SOD1*^{G37R} animals (see Extended Data Fig. 5e and Supplementary Tables 1 and 2).

Spinal SP delivery of AAV9–shRNA–*SOD1* after disease onset stops disease progression in *SOD1*^{G37R} mice.

Untreated *SOD1*^{G37R} mice developed disease onset at 312 d (Fig. 1f), and then progressed to mid-disease over the subsequent 5 weeks, characterized by reduced grip strength, presence of MFs and a 49% loss of α-motoneurons compared with wild-type nontransgenic mice (Fig. 5a–d; see Extended Data Fig. 6a,b,e). Disease reached the end-stage at 404 (±8) d in sham-operated or scrambled virus-injected animals (Fig. 5e), accompanied by loss of grip strength (Fig. 5f), presence of MFs (Fig. 5g), 81% (±5) of α-motoneurons and NeuN staining intensity in interneurons (Fig. 5g; see Extended Data Fig. 6c,f,g). In three of four animals treated after disease onset, however, disease did not progress after the injection of AAV9–shRNA–*SOD1*, with each escaping paralytic disease, and maintaining α-motoneuron number and NeuN + interneurons (see Extended Data Fig. 6d,f,g), normal righting reflex (Fig. 5e) and partial preservation of grip strength (Fig. 5f), and failure to develop MFs in two animals and only a moderate level in a third (Fig. 5h). Consistent with α-motoneuron protection and suppression of MFs in treated animals, qualitative analysis of NMJs in GCM showed normally appearing NMJs in treated animals, whereas widespread denervation was seen in sham-operated animals (see Extended Data Fig. 3d–g). Misfolded SOD1 was suppressed in the AAV9–shRNA–*SOD1*-treated, but not sham-treated, mice (see Extended Data Fig. 6c,d,h). Qualitative and quantitative analysis of inflammatory markers (glial fibrillary acidic protein (GFAP), Iba1, vimentin) showed no notable differences between treated and nontreated *SOD1*^{G37R} animals (see Extended Data Fig. 6i–w), presumably as a result of already ongoing neurodegeneration-induced inflammation at the time of treatment at age ~348 d.

Comparative analysis of mRNA transcripts in lumbar spinal cord between untreated *SOD1*^{G37R} animals in mid-stage disease (aged ~348 d) and untreated *SOD1*^{G37R} animals that had reached end-stage disease revealed 1,278 differentially expressed genes (593 upregulated and 685 downregulated) by the end-stage (see Extended Data Fig. 7a,c and Supplementary Table 3). In contrast, comparing differentially expressed genes between 348-d-old untreated *SOD1*^{G37R} animals and *SOD1*^{G37R} animals, treated at age ~348 d and surviving an additional 96 d, identified only a total of 113 differentially expressed genes (47 upregulated and 66 downregulated) (see Extended Data Fig. 7b,c and Supplementary Table 4).

Effective spinal SP cervical delivery of AAV9 in adult pigs and NHPs.

We next extended the translational potential of SP AAV9 delivery for human clinical use. First, a functional prototype of a human SP injection device was developed (Fig. 6a) and tested on adult pigs (n = 3; Gottingen–Minnesota pigs; body weight = 35–45 kg) with spinal

cord dimensions similar to those of adult humans33,34. Animals received 400 µl AAV9–UBI–*GFP* (1.4 × 1013 GC ml−1) into the cervical (C3) SP space (Fig. 6b). An additional cohort of pigs ($n = 3$) was injected intrathecally (C3 level—with 800 µl of the same vector). Three to six weeks after the injections, the distribution of green fluorescent protein (GFP)-expressing cells in the spinal cord and brain was determined using immunofluorescence.

SP injection produced GFP expression in neurons in cervical segments (Fig. 6c; and see Supplementary Fig. 7a-c). Retrograde infection of brain motor nuclei produced GFP expression in neurons of the tectospinal tract, nucleus ruber, reticular formation (pons and medulla oblongata), and pyramidal neurons in motor cortex innervating the forelimbs and hindlimbs (Fig. 6d–m; and see Extended Data Fig. 8a–f and Supplementary Fig. 7d–i).

In contrast, animals receiving a cervical IT injection showed only occasional GFP + α-motoneurons in the cervical spinal cord (see Supplementary Fig. 7j–l), with irregularly distributed cortical neurons expressing GFP and superficial cell populations in the medulla or brain stem, suggesting a regional diffusion of the vector from the cerebrospinal fluid or in the vicinity of penetrating arteries (see Supplementary Fig. 7m–r and Extended Data Fig. 9a–g). No GFP + neurons were detected in deep brain stem nuclei (see Supplementary Fig. 7p–r).

We next tested the spinal SP injection in NHPs. First, we determined the spread of subpially injected, fluorescence-tagged dextran (10,000 M_r; 300 µl) after C3 SP injection. During infusion, a rostro-caudal spread of blue-colored dextran in the SP space was seen (see Extended Data Fig. 10a–c). Next, we used AAV9-encoding *Rpl22*-3x*HA* (1.2 × 1013 GC ml −1) to identify the penetration of AAV9 vector into the cervical spinal cord. Adult animals (cynomolgus monkeys; $n = 2$) received an SP infusion of AAV9 vector (300 µl) between the C3 and C4 spinal segments. To compare the potency of subpially versus intrathecally delivered virus, the AAV9–*Rpl22*-3x*HA* vector (800 µl) was injected intrathecally ($n = 2$) into the C3 IT space. Animals were sacrificed at 48 h after AAV9–*Rpl22*-3x*HA* vector delivery. In the mouse study, we have demonstrated that Rpl22 protein is expressed in infected spinal cord neurons as soon as 24 h after vector delivery, and therefore allows a reliable identification of infected cells at early time points post-vector injection.

Subpially or intrathecally injected animals showed normal neurologic function after recovery from anesthesia and remained neurologically normal for 2 d of survival. In subpially injected animals, bilateral expression of Rpl22 was seen in neurons and glial cells between the C1 and C8 segments (see Extended Data Fig. 10d–l). No HA staining was detected in control spinal cord that had not been injected with vector (see Extended Data Fig. 10m,n). Qualitative and quantitative comparison between subpially and intrathecally injected animals showed between 45% and 80% of NeuN-positive neurons to be transduced in the subpially injected group (see Supplementary Fig. 8a,c,e,g), whereas only 2–3% of neurons were infected in the intrathecally injected animals (see Supplementary Fig. 8b,d,f,g).

Discussion

We have used a new spinal SP vector injection technique to deliver an shRNA–*SOD1*-silencing vector into the spinal cord parenchyma of adult presymptomatic or neurologically symptomatic *SOD1*^{G37R} ALS mice. We have demonstrated that a two-level (upper cervical and upper lumbar) spinal SP delivery of AAV9 results in a highly potent transduction of neuronal and glial cells in the entire spinal cord of adult mice. In addition, a retrograde transduction of supraspinal descending motor tracts (corticospinal, rubrospinal, reticulospinal) was observed20,21. Based on the well-characterized, widespread, neuronal degeneration observed in mutant *SOD1* rodent ALS models, including the loss of α-motoneurons, interneurons and descending motor tracts, we postulated that the shRNA–*SOD1*-silencing vector, once delivered into spinal cord by SP injection, would be highly effective in delaying disease onset or slowing disease progression if initiated either in adult presymptomatic individuals or sufficiently early in disease course after onset. Accordingly, we have demonstrated a long-term, almost-complete, functional and morphologic preservation of the neuraxis, including preservation of the NMJ if the treatment is initiated in adult presymptomatic animals, and potent preservation of residual neurologic function and persisting α-motoneuron survival if treatment is initiated after disease onset.

Prior studies have employed an identical silencing vector delivered systemically (intravenously) in early symptomatic *SOD1*^{G37R} mice; nevertheless, disease progression continued, reaching the end-stage with an extended survival of just under 3 months (ref. 16). No α-motoneuron quantification or electrophysiologic assays were used in that study; however, because the endpoint was defined by the loss of the righting reflex and correlated with reduced grip strength, it is likely that substantial neurodegeneration had occurred. In a more recent study using ICV injection of AAV9–shRNA–*SOD1* (the same construct as used in the present study), the *SOD1G93A* mouse lifespan was extended by 2 months if treatment was initiated at postnatal day 1. Treatment potency was substantially reduced, however, if the treatment was performed in 40-d-old animals, yielding only a 19-d extension of life14. A transient treatment effect has also been reported after a combined ICV plus systemic delivery of AAV10–U7–*hSOD1* in the same *SOD1G93A* model: vector delivery to 50-d-old animals produced a survival extension of 72 d (ref. 19). A most recent study by McCampbell et al.18 demonstrated that the ICV or lumbar IT delivery of an antisense oligonucleotide (ASO) targeting *SOD1* in presymptomatic animals extended survival by ~50 d in *SOD1G93A* rats and by ~40 d in *SOD1G93A* mice, although no quantitative histopathologic analysis to demonstrate spinal neuronal protection was performed. Collectively, systemic or ICV/IT delivery of AAV9–shRNA–*SOD1* in adult animals is not sufficient to target all neuronal and/or glial cell populations required to maintain long-term motor function.

In comparison, our SP injection approach administered to adult presymptomatic mice achieved a markedly improved long-term efficacy in mitigating neurodegeneration. All animals treated subpially with AAV9–shRNA–*SOD1* displayed normal neurologic function with no detectable disease onset for the duration of the study (an extension of a minimum of 156 d after typical onset). This functional effect corresponded with almost-complete protection of the motor neuraxis up to the NMJ. In addition, a potent suppression of disease progression was seen when animals were treated at a clinically defined symptomatic stage of

the disease. Thus, the SP vector delivery technique provides a high degree of consistency in terms of delivering a therapeutic vector at required titers throughout the entire spinal parenchyma in adult presymptomatic animals, and neurologically symptomatic animals as well. These characteristics can be of critical importance in designing well-controlled clinical protocols to be implemented in prescreened, presymptomatic patients or in a patient population at an early disease stage.

Although an allele-specific silencing effect would be desired in cases of autosomal dominant-linked mutations (such as mutations in the *SOD1* gene), current shRNA or ASO silencing technologies provide an overall decrease in both the mutated and the wild-type *SOD1* allele-induced synthesis. Accordingly, the guiding principle in using shRNA or ASO treatments is to diminish the mutated *SOD1* expression to below a toxic level, while maintaining a physiologic level of the wild-type *SOD1*. To accomplish this, a well-controlled delivery of silencing vectors at specific titers must be achieved throughout the entire spinal cord parenchyma. Based on the data from the present study, we believe that the use of a SP delivery technique can achieve these goals. Indeed, our direct comparison of the potency of subpially versus intrathecally delivered AAV9 vector has documented sharply improved potency of the SP approach in spinal cord parenchyma and brain motor centers, in adult mouse, pig and NHPs. Importantly, we have also demonstrated that, by using the intended human SP injection device, the SP injections can reliably be performed in animal species (adult pig) with spinal cord dimensions similar to those of adult humans, as well as in adult NHPs, and that there are no surgical procedure-related complications. Compared with direct parenchymal injection, the SP delivery is performed under full visual control and does not require a ‘blind’ parenchymal needle penetration. This substantially increases the safety of spinal vector delivery by eliminating a potential, spinal, parenchymal needle-caused spinal cord injury.

Collectively, our data demonstrate that the SP delivery of AAV9–shRNA–*SOD1* is a highly effective treatment approach to ameliorate clinical ALS symptoms associated with neuraxial mSOD1 protein accumulation, after treatment initiation in adult presymptomatic or neurologically defined symptomatic animals. The high consistency of the treatment effect across multiple treated mice, once treatment has been initiated at a different stage(s) of disease and documented favorable safety profile in large preclinical animal models injected with the human SP injection device, suggests that this approach can be an effective clinical strategy for the treatment of *SOD1*-mutation-linked ALS in humans. In addition, potent expression throughout the spinal cord in adult animals after SP AAV9 delivery indicates that this approach will probably be effective in delivering other therapeutic vectors, and may include mRNA- and DNA-editing systems.

Online content

Any methods, additional references, Nature Research reporting summaries, source data, extended data, supplementary information, acknowledgements, peer review information; details of author contributions and competing interests; and statements of code and data availability and associated accession codes are available at https://doi.org/10.1038/s41591–019-0674–1.

Methods

Viral vectors.

A self-complementary AAV (scAAV) construct expressing an shRNA-targeting human *SOD1* was previously described by Foust et al. (scAAV–*SOD1*–shRNA)16. The scAAV vector construct, expressing *Rpl22*-3x*HA* driven by the UBC promoter was made by DNA synthesis of the UBI promoter (1.2 kb) through *Rpl22*-3x*HA* (490 basepairs (bp)) or enhanced *GFP* (700 bp) and cloning it into an scAAV backbone plasmid. The scAAV9–*SOD1*–shRNA, scAAV9–UBI–*GFP* and scAAV9–UBI–*Rpl22*-3x*HA* vectors were produced by transient transfection of HEK293T cells with each vector plasmid, pRep2/Cap9 and pAd-Helper plasmid35. Plasmid pRep2/Cap9 was obtained from the Penn Vector Core. Cell lysates prepared at 72 h after transfection were treated with benzonase and viruses were purified by a combination of anion-exchange column chromatography and ultracentrifugation. Virus titers were measured using real-time qPCR to determine the GC number of the vector preparations, as a measure of the AAV particles with full GC (GC ml −1)36,37. The final concentration of the scAAV9–*SOD1*–shRNA was 5.6 × 1012 GC ml−1, scAAV9–UBI–*GFP* was 2.9 × 1013 GC ml−1 and scAAV9–UBI–*Rpl22*-3x*HA* was 2.3 × 1013 GC ml−1.

Animals.

Female and male *LoxSOD1*^{G37R} mice (on a C57BL/6 background), carrying a human mutant *SOD1*^{G37R} transgene, flanked by lox p sites by the action of Cre recombinase, were obtained from the Cleveland Laboratory (University of California San Diego (UCSD)). Cynomolgus macaques (*Macaca fascicularis*) with an average body weight of 2.5 kg (BTS Research) and mini-pigs (Göttingen–Minnesota mini-pigs) with an average weight of 40 kg (Czech Academy of Sciences) were used. The general health and body weight of all the animals were monitored on a regular daily basis during the whole experiment. All experiments were performed in accordance with the National Institutes of Health (NIH) Guidelines and approved by the UCSD, BTS Research and the Institute of Animal Physiology and Genetics, Czech Academy of Sciences Institutional Animal Care and Use Committee. See Nature Research Reporting Summary for details.

Experimental design.

Female and male *LoxSOD1*^{G37R} mice and their negative littermates were randomly divided into seven experimental groups: (1) *SOD1*^{G37R} mice sham operated (n = 14; 9 females and 5 males; at age ~120 d); (2) *SOD1*^{G37R} mice subpially treated with AAV9–shRNA–*SOD1* (n = 17; 9 females and 8 males; at age ~120 d); (3) *SOD1*^{G37R} mice subpially treated with AAV9–shRNA–*SOD1* (n = 4; 2 females and 2 males; at age ~348 d); (4) *SOD1*^{G37R} mice subpially treated with AAV9-empty (scrambled) vector or sham operated (n = 4; 3 females and 1 male; at age ~348 d); (5) *SOD1*^{G37R} nontreated mice (n = 4; 3 females and 1 male, survival till end-stage); (6) *SOD1*^{G37R} nontreated mice (n = 3; 1 female and 2 males perfused at age 348 ± 2 d); and (7) wild-type nontransgenic mice (n = 13; 5 females and 8 males). Baseline of general activity and grip strength were assessed before surgery and every week, starting 2 weeks after surgery until the sacrifice day. The virus spread and transgene expression efficacy after SP or IT injection was studied in adult B6 mice (SP: n = 4; IT: n =

4), in NHPs (SP: $n = 2$; IT: $n = 2$) and in mini-pigs (SP: $n = 3$; IT: $n = 3$), using the scAAV9–UBI–*Rpl22*-3x*HA* or scAAV9–UBI–*GFP* vectors with transgene expression analyzed at 48 h (scAAV9–UBI–*Rpl22*) or 4–6 weeks (scAAV9–UBI–*GFP*) after injection.

SP injections.

Mouse.—All surgical procedures were done under sterile conditions. A cervical (C3–C4) and lumbar (L1–L3) SP vector injection in mice was performed as previously described21. Briefly, mice were anesthetized with 2–3% isoflurane, the surgical area shaved and cleaned, and a skin incision made at the Th8–L1 or C2–C4 vertebral level. Under the dissecting microscope, a dorsal laminectomy of C3–C5 and Th13 vertebrae was performed and dura overlying C3–C4 and L1–L2 spinal segments cut open using a 30-G needle. The pia mater was then punctured using a 36-G pia-penetrating needle, followed by the insertion of a blunt 36-G injection needle containing the scAAV9 vector. Both the pia-penetrating and the SP injection needles were mounted on fine *XYZ* manipulator (SMM 100B, Narishige). Then, scAAV9–UBI–*Rpl22*-3x*HA*, scAAV9–UBI–*GFP* or scAAV9–shRNA–*SOD1* virus was injected into the cervical and/or lumbar SP space (10 µl of vector at each level injected over 60 s), using a 50-µl Hamilton syringe and digital infusion pump (Microinjector MINJ-PD, Tritech Research). Virus solution was mixed 1:1 with 5% dextran solution, to a final dextran concentration of 2.5% just before injection. After vector delivery, the needle was removed and muscle and skin closed using 3/0 Prolene. Before recovery from anesthesia, the animals received subcutaneous fluids, antibiotics and the initial dose of pain medication (Buprenex 0.05 mg kg−1).

NHPs and mini-pigs.—Adult NHP (*Macaca fascicularis*) and Göttingen–Minesotta mini-pigs were premedicated with ketamine (5–20 mg kg−1 intramuscularly) and induced with propofol (10 mg kg−1 intravenously). After endotracheal intubation, anesthesia was maintained with 1.5–2.5% isoflurane in 50% air:50% oxygen at a constant flow rate of 2 l min−1. The dorsal cervical area was then shaved and cleaned, and the animals were placed in a brain stereotaxic frame. The skin on the dorsal neck overlying the C1–C4 vertebrae was cut open, followed by a dorsal laminectomy of the C3 and C4 vertebrae. The dura mater was then cut open using a scalpel blade and the dorsal surface of the C3–C4 spinal segments exposed. Under the dissecting microscope a bent 27-G or 30-G needle (length 3–4 mm) was placed into the SP space in a rostrocaudal direction. Then scAAV9–UBI–*Rpl22*-3x*HA* (1.2 × 1013 GC ml−1, 300 µl) (NHPs) or scAAV9–UBI–*GFP* (1.4 × 1013 GC ml−1, 400 µl) (mini-pigs) was infused into the SP space at a rate of 1 µl per 5 s. Virus solution was mixed 1:1 with a 5% dextran solution to a final dextran concentration of 2.5% just before injection. After virus delivery, the needle was removed and muscle and skin closed using 3/0 Prolene. Before recovery, the animals received an antibiotic (cefazolin), pain medication (Buprenex), an immunosuppression drug (methylprednisolone (Depo-Medrol) 8 mg kg−1 intramuscularly) (single injection only) + tacrolimus (0.5 mg kg−1 d−1), delivered as a single subcutaneous injection of a 12-d releasable microsphere formulation (in mini-pigs only); they were then monitored until fully awake. Antibiotic and pain medication treatment continued for 2 d post-surgery survival.

IT injections.

Mouse.—Mice were anesthetized with 2–3% isoflurane, the surgical area shaved and cleaned, and a skin incision made at the Th8–L1 vertebral level. Under the dissecting microscope, a dorsal laminectomy of the Th13 vertebra was performed and dura overlying the L1–L2 spinal segments punctured using a 30-G needle. The blunt 36-G injection needle containing the scAAV9 vector was then inserted into the IT space using a fine *XYZ* manipulator (SMM 100B, Narishige).

NHPs and mini-pigs.—Adult NHPs (*Macaca fascicularis*) and mini-pigs (Gottingen–Minesotta) were anesthetized and the dorsal cervical area shaved and cleaned. The animals were placed in a brain stereotaxic frame. The skin on the dorsal neck overlying the C1–C4 vertebrae was cut open, followed by a dorsal laminectomy of the C3 and C4 vertebrae. The dura mater was punctured using a scalpel blade and, under the dissecting microscope, a bent 30-G needle (length 4 mm) was placed below the dura mater (into the IT space) in a rostrocaudal direction. Then scAAV9–UBI–*Rpl22*-3x*HA* (NHPs) or scAAV9–UBI–*GFP* (mini-pigs) was infused into the IT space at a rate of 1 μl per 5 s (800 μl for NHPs; 800 μl for mini-pigs). After virus delivery, the needle was removed and the dura mater, muscle and skin closed using 3/0 Prolene. Before recovery, the animals received an antibiotic (cefazolin), pain medication (Buprenex), an immunosuppression drug (methylprednisolone (Depo-Medrol) 8 mg kg−1 intramuscularly) (single injection) + tacrolimus (0.5 mg kg−1 d −1), delivered as a single subcutaneous injection of 12-d releasable microsphere formulation (in mini-pigs only); they were then monitored until fully awake. Antibiotic and pain medication treatment continued for 2 d post-surgery survival.

Grip-strength test.

A forelimb and hindlimb grip-strength test in mice was performed using a grip-strength meter (Columbus Instruments). Mice were held in front of a horizontal bar, in such a way that only the forelimb or the hindlimb paws could grasp the bar. To perform the test, animals were gently pulled back with a steady force until both paws released the bar. Peak tension in grams was recorded for five consecutive trials.

Open-field activity test.

An open-field test was performed for the assessment of the general motor activity (running distance) of animals before and after treatment. Briefly, an animal was placed in a 34 × 26 × 34 cm3 plastic box positioned in a dimly lit room with an overhead infrared video camera connected to PC-based tracking software (EthoVision XT 7.1, Noldus IT). The software monitored the actual animal movement based on a body-centered contrast subtracted from the background. All tested animals were released into the center of the plastic box (one animal per box), acclimatized to the room environment for 10 min and then continuously recorded for a total exploration time of 1 h. A total of six animals was recorded simultaneously at each recording session.

Onset and survival analysis.

Mice were weighed every week as an objective indirect measure of disease progression and functional motor tests (grip strength and open-field motor performance) were used to determine disease onset and progression. Disease onset was defined as a 20% decrease in grip strength (calculated from the peak grip strength) and by a 20% decrease in open-field running distance (calculated from the peak running distance). In nontreated $SOD1^{G37R}$ mice this stage is followed by progressive motor paralysis. The end-stage was defined by the loss of the righting reflex, when an animal could not right itself within 30 s when placed on its side. At this stage animals were euthanized and tissue collected for postmortem analysis.

Myogenic MEP recording.

Animals were anesthetized with propofol (50–100 mg kg−1, intraperitoneally) and two 30-G stainless steel-stimulating electrodes were placed subcutaneously, overlying the left and right motor cortices. MEPs were elicited by transcranial electrical stimulation with a pulse duration of 1 ms at 8.5 mA, using a DS3 constant current isolated stimulator (Digitimer). Responses were recorded from the GCM using 30-G platinum transcutaneous needle electrodes (distance between recording electrodes ~1 cm; Grass Technologies, Astro-Med). Recording electrodes were connected to an active headstage (3110W; Warner Instruments) and signal amplified (×100) using a DP-311 differential amplifier (Warner Instruments). The amplified signal was acquired by the PowerLab 8/30 data-acquisition system (ADInstruments) at a sampling frequency of 20 kHz, digitized and stored in a PC for analysis.

Resting EMG recording.

Animals were anesthetized with 2.5% isoflurane and the left forelimb and hindlimb were shaved. To record electromyographic (EMG) potentials, two 30-G platinum transcutaneous needle electrodes (Grass Technologies, Astro-Med) were placed into the triceps muscle and GCM with a distance between recording electrodes of ~1 cm in each muscle. Electrodes were connected to an active headstage (3110W; Warner Instruments), recorded signal amplified (×100) using the DP-311 differential amplifier (Warner Instruments), and digitized using the PowerLab 8/30 data-acquisition system (ADInstruments). The recorded signal was sampled at 20 kHz over 5 min and stored in a PC for analysis.

Hind paw, vagal nerve electrical stimulation and HR recording.

$SOD1^{G37R}$ mice at the presymptomatic stage (age ~116–170 d, $n = 8$) or the symptomatic stage (age ~415 d, $n = 1$) and wild-type animals ($n = 9$) were anesthetized with 1.5% isoflurane via a facemask. For all electrocardiographic (EKG) and heart rate (HR) recordings, 30-G platinum needle electrodes were inserted subcutaneously according to the EKG scheme—left foreleg, right foreleg and left rear leg. For right hind paw stimulation, a pair of 30-G platinum needle electrodes was inserted into the interosseous muscles between the fourth and fifth, or the first and second, metatarsal muscles of the right hind paw. The baseline values of HR were measured 1 min before stimulation. The paw was then stimulated using square current pulses (10 mA, 2 ms) delivered to the electrode at frequencies of 10 Hz by a DS3 constant current isolated stimulator (Digitimer). The duration

of the stimulus train was 20 s, and the maximal HR responses to electrical stimulation were determined. Responses were recorded with an A/C-coupled differential amplifier (Model DP-311, Warner Instrument). Amplified signal (×100) was acquired by the PowerLab 8/30 data-acquisition system (ADInstruments) at a sampling frequency of 20 kHz, digitized and stored in a PC for analysis. For right cervical vagus nerve stimulation, an incision was performed in the ventral side of the neck of the mice to isolate the right cervical vagal nerve. The nerve was placed on a pair of bipolar silver hook electrodes and electrically stimulated using square current pulses (100 μA, 1 ms), delivered at frequencies of 5 Hz and 10 Hz, using a DS3, constant current, isolated stimulator (Digitimer). The duration of the stimulus train was 20 s, and evoked frequency-dependent decreases in HR responses to electrical stimulation were measured. Responses were recorded with an A/C-coupled differential amplifier (Model DP-311, Warner Instrument). An amplified signal (×100) was acquired by the PowerLab 8/30 data-acquisition system (ADInstruments) at a sampling frequency of 20 kHz, digitized and stored in a PC for analysis.

Tissue collection.

Mice were euthanized with pentobarbital (100 mg kg−1) and perfused with 20 ml ice-cold phosphate-buffered saline (×1 PBS). The spinal cord, brain, sciatic nerve, muscle, Th2–Th4 sympathetic ganglia, L3 dorsal root ganglion and liver were then dissected. The spinal cord was then divided into cervical, thoracic and lumbar segments, and each segment divided into four pieces. The two rostral pieces, brain, muscle and thoracic sympathetic ganglia, and L3 dorsal root ganglion were dropped into ice-cold, freshly prepared fixative (4% paraformaldehyde (PFA) dissolved in 0.15 M sodium phosphate buffer, pH 7.4). Samples were then postfixed overnight (muscle was postfixed for 3 d) at 4 °C and cryoprotected for 72 h in 30% sucrose until immunohistochemistry and FISH had been performed. The other two pieces of spinal cord and the liver were flash frozen in dry ice and saved for qPCR, RNA-sequencing (RNA-seq) and western blot analysis.

Animals used for postmortem, spinal cord, MRI volumetric analysis, and spinal cord and sciatic nerve axonal quantification (plastic sections), were euthanized with pentobarbital and the whole body perfused with 20 ml ice-cold ×1 PBS followed by 20 ml freshly prepared fixative (4% PFA dissolved in 0.15 M sodium phosphate buffer, pH 7.4). After MRI was completed spinal cord and sciatic nerves were kept in 4% PFA until further processing.

Animals used for HR, EKG and vagus nerve recordings were euthanized after the electrophysiologic experiment and perfused with 20 ml ×1 ice-cold PBS. The right vagus nerve, spinal cord and Th2–Th4 sympathetic ganglia were dissected and dropped into ice-cold, freshly prepared fixative (4% PFA dissolved in 0.15 M sodium phosphate buffer, pH 7.4), Spinal cords and Th2–Th4 sympathetic ganglia were then postfixed overnight at 4 °C and cryoprotected for 72 h in 30% sucrose, until immunohistochemistry could be performed, whereas the vagus nerve was kept in 4% PFA until further processing.

NHPs and mini-pigs were euthanized with pentobarbital (100 mg kg−1) and perfused with 1,000 ml (NHPs) or 3,000 ml (mini-pigs) of heparinized saline followed by 1,000 ml (NHPs) or 3,000 ml (mini-pigs) of 4% PFA in PBS. The spinal cords and brains were dissected and postfixed in 4% PFA in PBS overnight at 4 °C.

Immunohistochemistry.

Cryoprotected spinal cord, brain, muscle or thoracic sympathetic ganglia tissue were embedded in Optimal Cutting Temperature (OCT) matrix compound (Tissue-Tek, Sakura Finetek), frozen with dry ice and mounted in the cryostat. Sections were cut from the spinal cord, brain stem, brain and muscle (30-μm thickness) or cervical sympathethic ganglia (15-μm thickness). Free-floating sections were washed three times in PBS with 0.3% Triton-X100 followed by a blocking step with 4% serum in ×1 PBS with 0.3% Triton-X100 for 1 h. Sections were then incubated in the primary antibodies (in blocking solution) overnight at 4 °C. The following day, the sections were washed three times with ×1 PBS with 0.3% Triton-X100, and incubated with secondary antibody in PBS, 0.3% Triton-X100 for 1 h at room temperature. Sections were mounted on slides, dried at room temperature and cover-slipped in ProLong Gold antifade mounting medium, with DAPI (Invitrogen). The following primary antibodies and dilutions were used: misfolded hSOD1 (mouse, Medimabs clone B8H10, no. MM-0070-P, dilution 1:500), NeuN (rabbit, Millipore-Sigma, anti-NeuN, no. ABN78, dilution 1:1000), ChAT-choline acetyltransferase (goat, Millipore-Sigma, anti-choline acetyltransferase, no. AB144P, dilution 1:100), GFAP−Cy3 (mouse, Millipore-Sigma, clone G-A-5, no. C9205, dilution 1:1,000), Iba1 (rabbit, Wako clone NCNP24, no. 019–19,741, dilution 1:1,000), GFP (chicken, Abcam, anti-GFP no. AB13970, dilution 1:1,000), HA (mouse, Millipore-Sigma, clone HA-7, monoclonal anti-HA no. H9658, dilution 1:500), α-BTX (α-bungarotoxin, Alexa Fluor 555 conjugate, Invitrogen, no. B35451, dilution 1:500), Synapsin (rabbit, Milipore-Sigma, anti-synapsin I, no. S193, dilution 1:50), neurofilament (chicken, Milipore-Sigma, anti-neurofilament H, no. AB5539, dilution 1:500), tyrosine hydroxylase (rabbit, Milipore-Sigma, anti-tyrosine hydroxylase, no. AB152, dilution 1:500). For detection of primary antibodies, donkey anti-rabbit, anti-mouse, anti-chicken or anti-goat Cy3, Cy5 or Alexa 488-conjugated secondary antibodies (Jackson ImmunoResearch), diluted 1:1,000, were used. See Nature Research Reporting Summary for details.

Semithin section preparation and staining.

Segments of sciatic nerve and spinal cord were embedded in the protein matrix as described by Herzog et al.38, to facilitate the preparation of 1-mm-thick slabs for further processing. Briefly, before embedding, the tissue was blotted dry and pinned on to a silicone mold. The mold was then filled with glutaraldehyde-polymerized protein matrix, prepared as follows: the stock solution was prepared by dissolving 0.75 g gelatin (150 bloom, BDH Ltd) and 30 g sucrose in 50 ml warm 0.1 M PBS. Separately, 57 g chicken egg albumin (BDH Ltd) was dissolved in 100 ml of 0.1 M phosphate buffer. Both these solutions were mixed and filtered through muslin. For embedding, 9 parts of the gelatin:albumin solution were mixed with 1 part of ice-cold 25% glutaraldehyde. After stirring quickly, the solution was poured over the specimen and allowed to polymerize at room temperature. After approximately 10 min, the hardened matrix with the embedded tissue was removed from the mold and stored in 0.1 M phosphate buffer. The embedded tissue was placed into a metallic tissue matrix (TM-1000 10 × 10 mm2 chamber with 1-mm slices; ASI Instruments) and cut with a microtome blade into 1-mm thick slabs. Individual slabs were postfixed in 2% osmium tetroxide for 2 h and embedded into Durcupan resin. The 1- to 2-μm-thick sections were cut with a sliding microtome (Leica SM2010R) using a special blade for hard materials (Feather N35HR). The

sections were teased on to gelatin-coated slides from 90% ethanol and dried at 60 °C. The sections were stained with toluidine blue and cover-slipped with Poly-Mount (Polysciences, Inc.).

Sciatic nerve and spinal cord lateral funiculus quantification.

Stained transverse sections taken from the sciatic nerve and spinal cord were scanned using a digital pathology slide scanner Aperio AT2 (Leica) at maximal resolution (×40). In a digital image, a square (0.3 × 0.3 mm2) was drawn in the lateral funiculi of the spinal cord. The morphometric analysis of myelinated axons was performed both in the sciatic nerve and within the drawn square on the lateral funiculus using customized, object-analyzing software (NeuroCounter). The software automatically analyses the digital image and recognizes myelinated axonal profiles as individual objects. The software allows manual correction of missing or incorrectly detected objects. The test version of NeuroCounter is available for download free of charge from http://www.saske.sk/~tomori/software/NeuroCounter. The results of the analysis include the total number of axons and the size of each individual axon.

FISH.

A paired double-*Z* oligonucleotide probe against target *hSOD1* RNA was predesigned and commercially available from RNAscope (Hs-SOD1-nonXMm; NM_000454.4, 14 pairs, 9–798 nucleotides). Pre-fixed tissue was embedded in OCT (Tissue-Tek Sakura Finetek), frozen in dry ice and mounted in the cryostat. Sections from the spinal cord were cut at a thickness of 15 μm and directly mounted on Superfrost Plus slides (Thermo Fisher) and left overnight at room temperature to dry. The following day, RNA FISH was performed using the RNAscope Multiplex Fluorescent v.2 (no. 323100), following the fixed frozen tissue protocol according to the manufacturer's instructions. Briefly, the tissues were treated with peroxidase hydrogen blocker before boiling at 98–100 °C in a pretreatment solution for 10 min. Protease plus was then applied for 30 min at 40 °C. The target probe (Hs-SOD1-nonXMm) was prediluted 1:50 and hybridized for 2 h at 40 °C, followed by a series of signal amplification and washing steps. All incubation steps at 40 °C were performed in a HybEZ Hybridization System. Hybridization signals were detected by a chromogenic reaction using red chromogen (PerkinElmer TSA Plus Cyanine 3 System). RNA-staining signal was identified as red punctate dots and clusters. RNA quality was evaluated for each sample using RNAscope 3-plex Positive Control Probe—mouse specific containing the housekeeping gene cyclophilin B (*PPIB*), RNA polymerase subunit IIA (PolR2A) and ubiquitin C (UBC). Negative control background staining was evaluated using a probe specific to the bacterial *dapB* gene (RNAscope 3-plex Negative Control Probe).

Fluorescence microscopy.

Fluorescence images were captured using an immunofluorescence microscope (Zeiss AxioImager M2 Microscope, Carl Zeiss) at the same exposure settings and fluorescent lamp intensity using the ×10 and ×20 objectives and the Stereo investigator software (MBF Bioscience). Mosaic images were captured from complete spinal cord sections or ventral and dorsal horns independently, at the desired wavelength or spectrum of light from each independent channel to obtain the best focal plane. ImageJ software was used to perform the desired merge for each double- or triple-stained section. Using an apotome accessory tool

from Zeiss microscope, we created high magnification images in *Z* stack of 30 optical sections in 0.3- to 0.5-μm steps. Identical settings were kept across all sections and microscopy sessions. Complete *Z* stack images were loaded into ImageJ and average intensity *Z* projections were generated. High magnification confocal images (1,024 × 1,024 pixels) were captured using a Fluoview FV1000 microscope (Olympus) with ×40 and ×60 objectives. Confocal images were then processed using Olympus FV10-ASW Viewer software where *Z* projections from 30–50 optical sections in 0.2- to 0.5-μm steps were compiled. Identical settings were kept across all sections and microscopy sessions. See Nature Research Reporting Summary for details.

α-Motoneuron quantification.

Transgenic $SOD1^{G37R}$ mice (shRNA–*SOD1* treated and sham operated) and their negative littermates were used ($n \geq 6$ animals for each group). Spinal cord sections (30 μm transverse, free floating) taken from cervical (C1–C3), thoracic (Th1–Th4) and lumbar (L2–L4) regions were stained side by side with NeuN and ChAT antibody. Four sections per segment for each region and animal with at least 230 μm spacing were selected for quantification. Quantification was done using a Zeiss AxioImager M2 microscope and ImageJ software. Only α-motoneurons (≥400 μm2 surface area) with visible nucleoli and prominent terminal C buttons on the cell bodies were counted.

Misfolded SOD1 signal quantification.

Transgenic $SOD1^{G37R}$ mice (shRNA–*SOD1* treated and sham operated) and their negative littermates were used ($n \geq 6$ animals). Spinal cord sections (30 μm transverse, free floating) from lumbar (L2–L4) and cervical regions (C1–C3) were stained side by side with the B8H10 antibody. Four sections per segment for each animal and region, with at least 230 μm spacing, were selected for quantification. Virtual tissue images of whole transverse sections were acquired at ×10 using a Zeiss AxioImager M2 microscope and Stereo Investigator software (MBF Biosciences). Identical camera and fluorescent light source settings were used across all sections and microscopy sessions. The mean gray value of B8H10 antibody signal was then measured using ImageJ software.

NeuN and glia quantification.

Transgenic $SOD1^{G37R}$mice (shRNA–*SOD1* treated and sham operated) and their negative littermates were used ($n \geq 6$ animals). Spinal cord sections (30 μm transverse, free floating) from the lumbar region (L2–L4) were stained side by side with NeuN, GFAP and Iba1 antibodies. Four sections per segment for each animal with at least 230 μm spacing were selected for quantification. Virtual tissue images of whole transverse sections were acquired at ×10 using a Zeiss AxioImager M2 microscope and Stereo Investigator software (MBF Biosciences). Identical camera and fluorescent light source settings were used across all sections and microscopy sessions. Using ImageJ software the mean gray value of the GFAP and Iba1 signal was measured in the whole gray matter, and the NeuN mean gray value was taken from laminae IV–VII.

Rpl22–3xHA quantification.

Spinal cord sections taken from SP ($n = 2$) and IT ($n = 2$) injected NHPs (scAAV9–UBI–*Rpl22*-3x*HA*) were used. Cervical sections (30 μm transverse, free floating) from C1, C2, C4, C5, C7 and C8 segments were stained side by side with NeuN and HA antibodies. Three sections per segment for each animal with at least 230 μm spacing were selected for quantification. Virtual tissue images of whole transverse sections were acquired at ×10 using a Zeiss AxioImager M2 microscope and Stereo Investigator software (MBF Biosciences). Identical camera and fluorescent light source settings were used across all sections and microscopy sessions. Using ImageJ software the number of NeuN+ and Rpl22-HA+ neurons were quantified using the particle analyzer keeping a size (pixel2) of 0.5–infinity and a circularity of 0.2–1.00.

Real-time qPCR.

Total RNA was isolated using TRIzol reagent (Invitrogen). RNA was quantified by spectrophotometry using an absorbance of 260 nm and the sample purity ratios were calculated (260/280 nm). For complementary DNA synthesis, RNA was subjected to reverse transcription with random hexanucleotides and the M-MLV reverse transcriptase (Invitrogen), following the manufacturer's instructions. The qPCR for human *SOD1* was performed on 250 ng total RNA (1:50 cDNA) using the iQSYBR Green supermix (Bio-Rad) with the iCycler iQ5 multicolor real-time-PCR detection system, according to the manufacturer's instructions and collected by the Bio-Rad IQ5 optical system software v.2.1.97.1001. The *Mus musculus* ribosomal protein S9 (Rps9, NM_029767) gene was also measured as an endogenous reference. The probe sequences used are the following: DD90-*hSOD1* exon 2: forward: GAAGGTGTGGGGAAGCATTA; DD91-*hSOD1* exon 3 reverse: CCCACCGTCTTTTCTGGATA; *mRPS9*: forward: GACCAGGAGCTAAAGTTGATTGGA, and reverse: GCGTCAACAGCTCCCGGGC.

Western immunoblot.

Tissues were homogenized in ice-cold lysis buffer (0.2% NP-40, ×1.5 Mini cOmplete EDTA free, 0.02 M β-mercaptoethanol and 10 mM phenylmethylsulfonyl fluoride), centrifuged at 4 °C and the supernatant fraction was transferred to a clean tube. Protein concentration was measured using Lowry's assay (D protein assay, Bio-Rad). Protein 7 μg was resolved by denaturing with 4–12% Bis-Tris Plus Gels (Invitroge Bol) and transferred to polyvinylidene difluoride membranes. The membranes were blocked with 5% nonfat milk in Tris-buffered saline at pH 7.4 (20 mM Tris, 150 mM NaCl and distilled H2O) with 1% Tween, and they were incubated with anti-SOD1 (rabbit, Abcam, no. 16831, dilution 1:10,000); to detect primary antibody, an anti-rabbit immunoglobulin (Ig) G, horseradish peroxidase-linked antibody (Cell Signaling, no. 7074S, dilution 1:10,000) was used. The signal of the SOD1 (17 kDa) was detected using an enhanced chemiluminescence detection system according to the manufactureŕs instructions (SuperSignal West Femto Maximum Sensitivity Substrate, catalog no. 34095, Millipore). The images were taken using the ChemiDoc MP imaging system and ImageJ lab v.5.0 build 18. Blots were stripped and incubated with a monoclonal antibody directed against β-actin (mouse, GeneTex, clone GT5512, no. GTX 629630, dilution 1:10,000). For detection of primary antibody, an anti-mouse IgG horseradish

peroxidase-linked antibody (Cell Signaling no. 7076S, dilution 1:10,000) was used. β-Actin was used as an internal control to normalize SOD1 protein expression levels.

RNA-seq.

RNA isolation.—Total RNA was isolated from flash frozen cervical and lumbar mouse spinal cords using the Qiagen RNeasy Plus Mini kit. RNA 1–2 μg was isolated from each sample, with RNA integrity number scores of approximately 9.0, as determined by TapeStation analysis (Agilent). The mRNA-seq libraries were prepared using the Illumina TruSeq Stranded mRNA Library kit, and sequenced with 75-bp reads (SR75) on the Illumina HiSeq4000 platform. The number of animals used for sequencing experiments was as follows: wild-type nontransgenic ($n = 5$), untreated *SOD1* end-stage disease ($n = 3$), sham-treated *SOD1* end-stage disease ($n = 4$), presymptomatic shRNA-treated *SOD1* ($n = 4$), untreated *SOD1* mid-stage disease ($n = 3$) and postsymptomatic shRNA-treated *SOD1* ($n = 3$).

Alignment and expression quantification.

Single-end 75 base reads (average 20 million reads per sample) were aligned to the mouse genome (mm10) using STAR. Successfully aligned reads were then quantified using Kallisto against the Gencode (M17) transcript database. Reads that failed to align to the mouse genome were quantified using Kallisto against the Gencode v.28 transcript database for humans to quantify levels of human *SOD1* within the mouse samples. Human *SOD1* was appended to the mouse gene expression tables and included in the downstream analysis.

Differential expression and clustering.

Differential expression was performed using the negative binomial test provided with the edgeR package in R. Pergene dispersions were estimated using DESeq, DESeq2 and edgeR, retaining the median estimated dispersion level from the three. Dispersions were calculated on the full gene expression table and sample conditions were provided to each dispersion estimation function, resulting in a condition aware estimate. This single estimate was provided as the dispersion for each individual, pairwise, differential expression test to keep all tests within a common dispersion context. Genes with fewer than 10 reads in both conditions were included in the differential expression tests; however, they were not included in the results and were not posthoc corrected. Potential batch effects were removed using the removeBatchEffect function in the limma package in R. Posthoc correction was performed on all tested genes' raw *P* values using the Benjamini–Hochberg correction. Genes were considered significantly differentially expressed if their posthoc corrected *P* values were <0.05.

Differentially expressed genes (between wild-type nontransgenic and *SOD1* end-stage disease animals) were considered to be 'corrected' after treatment if the expression of the gene in shRNA-treated *SOD1* animals was no longer notably different from the wild-type animals. Genes were considered 'partially corrected' if there was an important change in gene expression between treated and untreated *SOD1* animals, but there was still a notable difference in expression between the treated and the wild-type animals. 'Uncorrected' genes showed no important change in expression between shRNA-treated and untreated *SOD1*

animals. ‘Overcorrected’ genes exhibited differential expression between shRNA-treated *SOD1* animals and wild-type nontransgenic animals, but in the opposite direction to the change between untreated *SOD1* and wild-type nontransgenic animals. ‘Sham-affected’ genes exhibit differential expression between sham-treated and untreated *SOD1* animals.

The clustering dendrogram was generated by pairwise euclidean distances between samples. The genes included in the distance measurement were those found to be strongly associated with the experimental conditions via edgeR’s GLM functionality, testing the overall reduction of residual variance between a model that included the experimental conditions and a null model that was blind to the conditions. The dendrogram was created with the ‘hclust’ function in R using the ‘ward.D’ algorithm. A minimum spanning tree plot was generated using the DDRTree dimension reduction in Monocle.

Gene ontology.

Gene ontology enrichment was performed using the gene ontology annotations for molecular function, biological process and cellular component, as well as the KEGG and REACTOME databases. Gene lists from differential expression tests were tested for term enrichment against the background of all genes included in the differential expression tests using a hypergeometric test. Terms were clustered by computing pairwise similarity scores based on shared gene names associated with the terms. The kappa statistic described in the DAVID Bioinformatics Resources was used as a similarity score. A 10-nearest neighbors network was constructed and clustered using the ‘infomap.community’ function provided in the igraph package for R.

MRI.

Ex vivo, high-resolution MRI of the mouse lumbar spinal cords.—For transgenic $SOD1^{G37R}$ mice—shRNA–*SOD1* treated ($n = 3$); sham operated ($n = 4$) and wild-type nontransgenic control ($n = 3$)—imaging was performed using a 9.4-T AVHD, 400-MHz Bruker microimaging system with ParaVision 6 software (Bruker Biospin). The mice were perfused with 4% PFA solution and intact spinal columns, including vertebral bone, were harvested and placed in the PFA solution for >3 d before MRI. The vertebral columns were cut at the intervertebral disks between Th8 and L5 to contain spinal cord lumbar enlargement. Spinous and transverse processes were trimmed, and intact vertebral column segments were placed into 5-mm-diameter glass nuclear magnetic resonance tubes. MRI data were acquired using a T2-weighted, three-dimensional, spin-echo pulse sequence with a multi-echo train with parameters: 4 averages, echo spacing (echo time) = 10 ms, 4 echo images, repetition time = 935 ms, 300 × 90 × 90 matrix, the field of view = 15 × 4.5 × 4.5 mm3 and 50-μm isotropic voxel resolution. The total scan time was approximately 8.5 h per sample. Post-processing image analyses were performed by manual segmentation of gray and white matter boundaries, slice by slice, using Amira 3D software v.6.0.1 (Thermo Fisher Scientific). From these data, we calculated the total volumes of gray and white matter in lumbar enlargement (1-cm spinal cord length) and performed three-dimensional renderings for display in Amira. See Nature Research Reporting Summary for details.

Statistical analysis.

All data were expressed as mean ± s.e.m. or s.d. and plotted using GraphPad Prism v.5. For analysis of normally (parametric) distributed data, the mean values from individual groups were compared using either an independent sample unpaired, two-tailed, Student's *t*-test, one-way analysis of variance (ANOVA) or repeated measurements of two-way ANOVA with a posthoc test and *P* values adjusted for multiple comparisons, depending on the total number of treatment groups. For non-normally (nonparametric) distributed data, the median values from individual groups were compared with either the Steel–Dwass posthoc test, or a Kruskal–Wallis test and Mann–Whitney U-test, with Bonferroni's adjustment for multiple comparisons. Disease onset and righting reflex analysis between groups were performed using the Kaplan–Meier survival, two-sided, log-rank test. Exact *P* values are described in each figure and between the indicated groups.

Reporting summary.

Further information on research design is available in the Nature Research Reporting Summary linked to this article.

Data availability

All requests for raw and analyzed data and materials are promptly reviewed by the University of California San Diego (Material Transfer office) to verify whether the request is subject to any intellectual property or confidentiality obligations. Any data and materials that can be shared will be released via a Material Transfer Agreement. All raw and analyzed sequencing data can be found at the National Center for Biotechnology Information Sequence Read Archive (accession number GSE135539).

Code availability

The data of this study were analyzed with standard software that is already available and do not require a custom code.

Extended Data

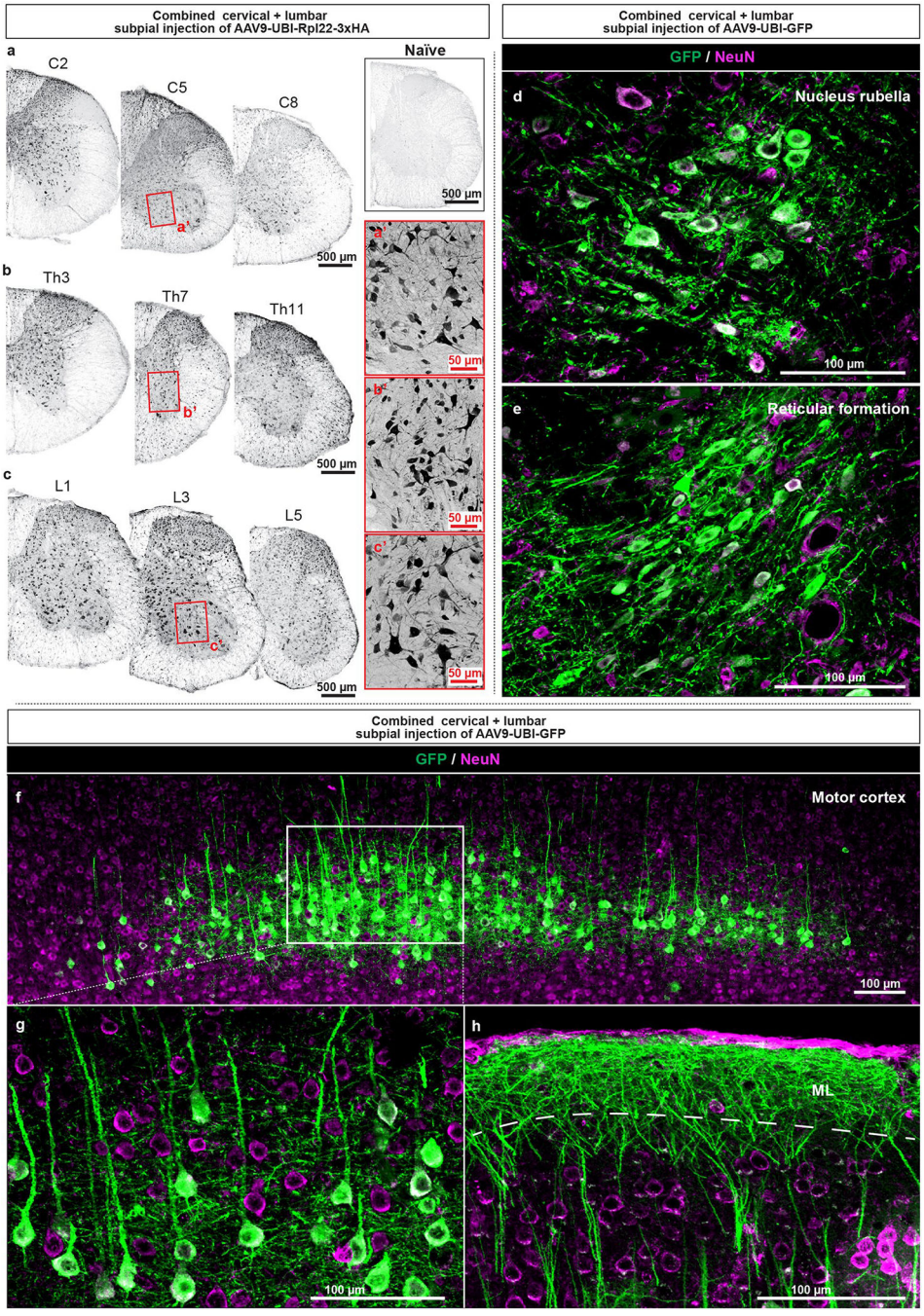

Extended Data Fig. 1 |. Potent Rpl22 and GFP protein expression throughout the spinal cord and brain motor centers after subpial AAV9-mediated delivery in adult wild-type (C57BL/6) mice. **a-c**, Wide-spread Rpl22 protein expression in cervical, thoracic and lumbar spinal cord at 24 h after a combined cervical-C4 (10 µl) and lumbar–L1 (10 µl) AAV9-UBI-*Rpl22*-3x*HA* delivery. Sections were stained with the anti-HA antibody (black signal). **d-h**, An intense retrograde transduction-induced GFP expression in (**d,e**) nucleus ruber and (**f-h**) motor cortex at 14 days after a combined cervical (10 µl) and lumbar (10 µl) AAV9-UBI-*GFP*

injection. A representative images from at least 4 individual animals are shown. ML, molecular layer.

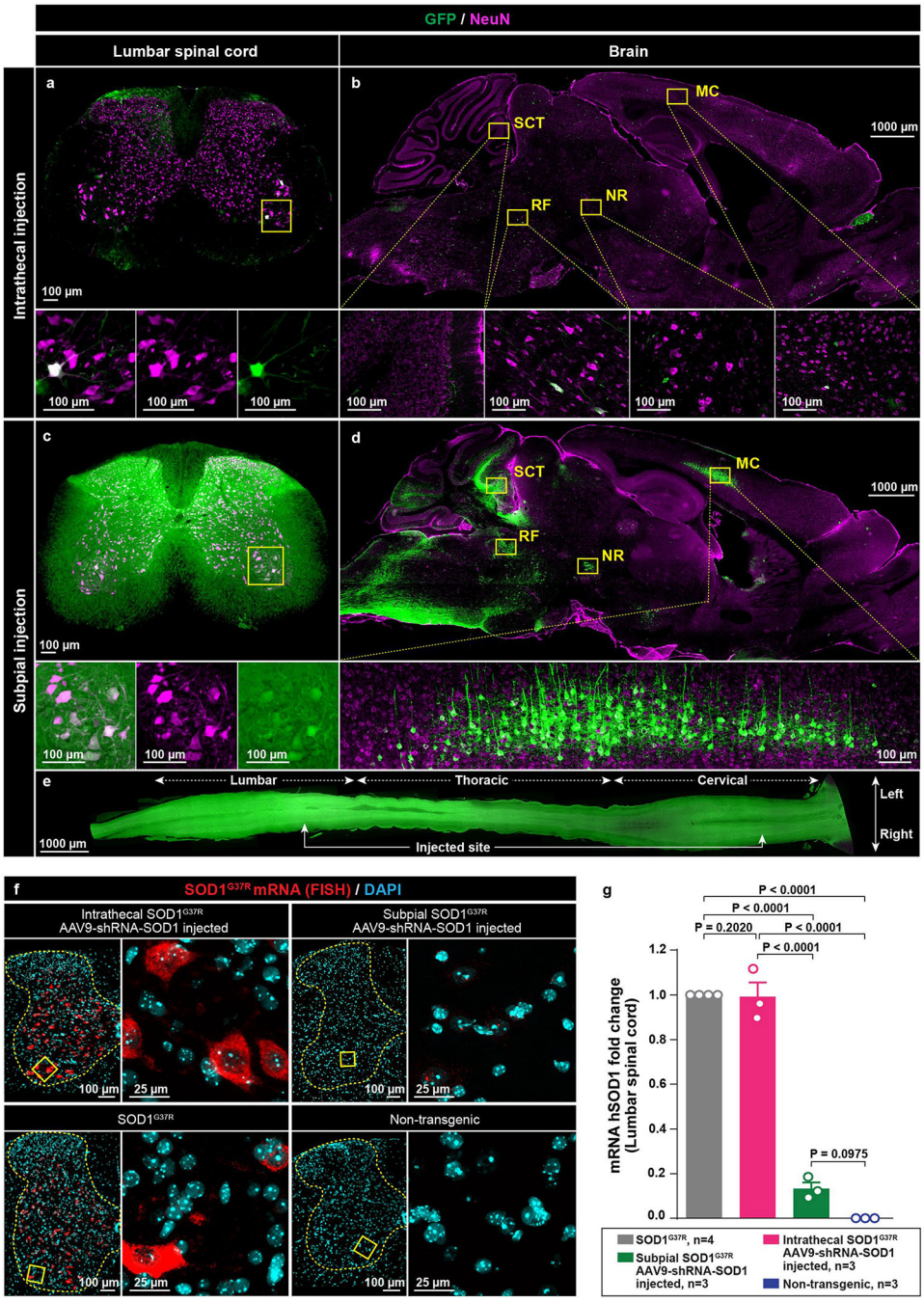

Extended Data Fig. 2 |. Potent gene expression or suppression of mutant SOD1^{G37R} expression in spinal parenchyma after spinal subpial, but not intrathecal, AAV9 delivery.

a-e, GFP expression after (a,b) intrathecal or (**c-e**) subpial injection of AAV-UBI-*GFP*. **a,b**, Only some α-motoneurons and occasional neurons in brain stem show GFP positivity following intrathecal injection. **c-e**, GFP expression throughout the entire length of spinal cord, spinocerebellar tract terminals (SCT) and brain motor centers (reticular formation-RF,

nucleus ruber-NR, and motor cortex-MC) in animals subpially-injected with AAV9-UBI-*GFP* at single cervical (C4) and lumbar (L1) sites. **e**, Longitudinal spinal cord section demonstrating expression of GFP throughout the spinal cord after subpial AAV9-UBI-*GFP* delivery. A representative images from at least 3 individual animals per experimental group are shown. **f**, **g**, Mutant $SOD1^{G37R}$ RNA levels measured by FISH or Q-PCR (four weeks after AAV injections) in the lumbar spinal cord in $SOD1^{G37R}$ mice injected subpially or intrathecally with AAV9-shRNA-*SOD1*. Highly potent (over 80%) suppression of $SOD1^{G37R}$ mRNA in subpially-vector-injected animals can be seen with FISH and was measured with Q-PCR. No significant silencing effect in intrathecally-injected animals was detected. (f) A representative images from at least 3 individual animals per group are shown. Data are expressed as mean ± S.E.M. ($SOD1^{G37R}$, n = 4; Subpial $SOD1^{G37R}$ AAV9-shRNA-*SOD1*-treated, Intrathecal $SOD1^{G37R}$ AAV9-shRNA-*SOD1*-treated and wild-type nontransgenic, n = 3 per group). Each dot represents an individual animal. Statistical significance was determined with one way ANOVA followed by Bonferroni post hoc test (ANOVA < 0.0001, F = 338.6). P values are shown between the indicated groups.

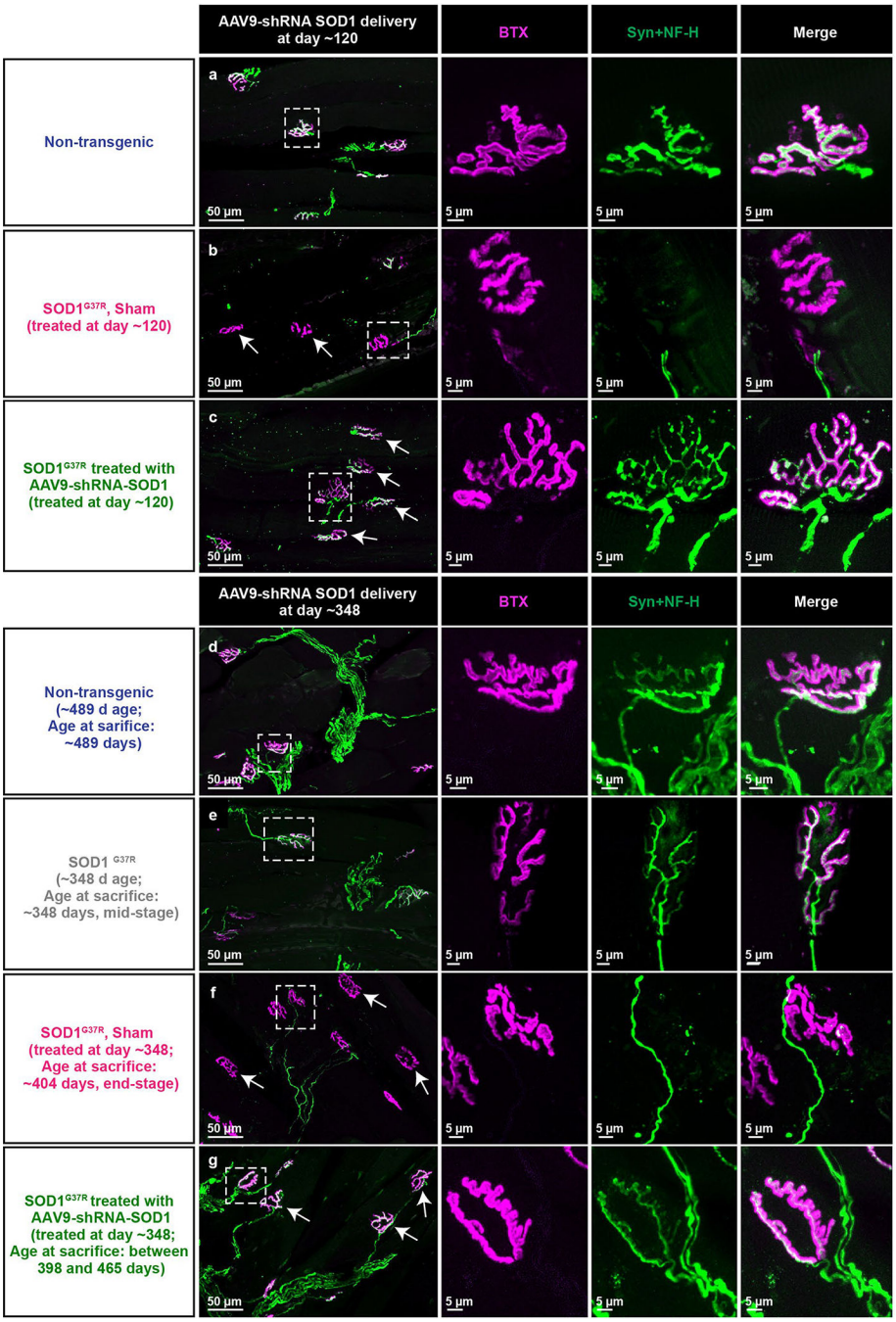

Extended Data Fig. 3 |. Preservation of neuromuscular junctions (NMJs) in gastrocnemius muscle in *SOD1*^{G37R} mice treated before or after disease onset with AAV9-shRNA-*SOD1*.

a-c, Several normally-appearing NMJs triple-stained with BTX/SYN/NF-H and which are similar to (**a**) wilde-type nontransgenic animals can be seen in (**c**) *SOD1*^{G37R} animals treated with AAV9-shRNA-*SOD1* at age of 120 days and analyzed at age ~470 days. **b**, Denervated (BTX + /SYN +, but NF-H negative) NMJs are found in sham-operated *SOD1*^{G37R} animals. **d,e**, Compared to wild-type nontransgenic animal (**d**) a partial denervation (loss of BTX + /SYN + /NF-H +) is seen in *SOD1*^{G37R} animals at age of ~348

days (**e**). **f,g**, Compared to end stage sham-operated animals which show extensive loss of NMJs (**f**) the innervation is maintained in *SOD1*^{G37R} animals treated after disease onset (at age ~348 days) with AAV9-shRNA-*SOD1* and analyzed at age between 398–465 days (**g**). A representative images from at least 3 individual animals per experimental group are shown.

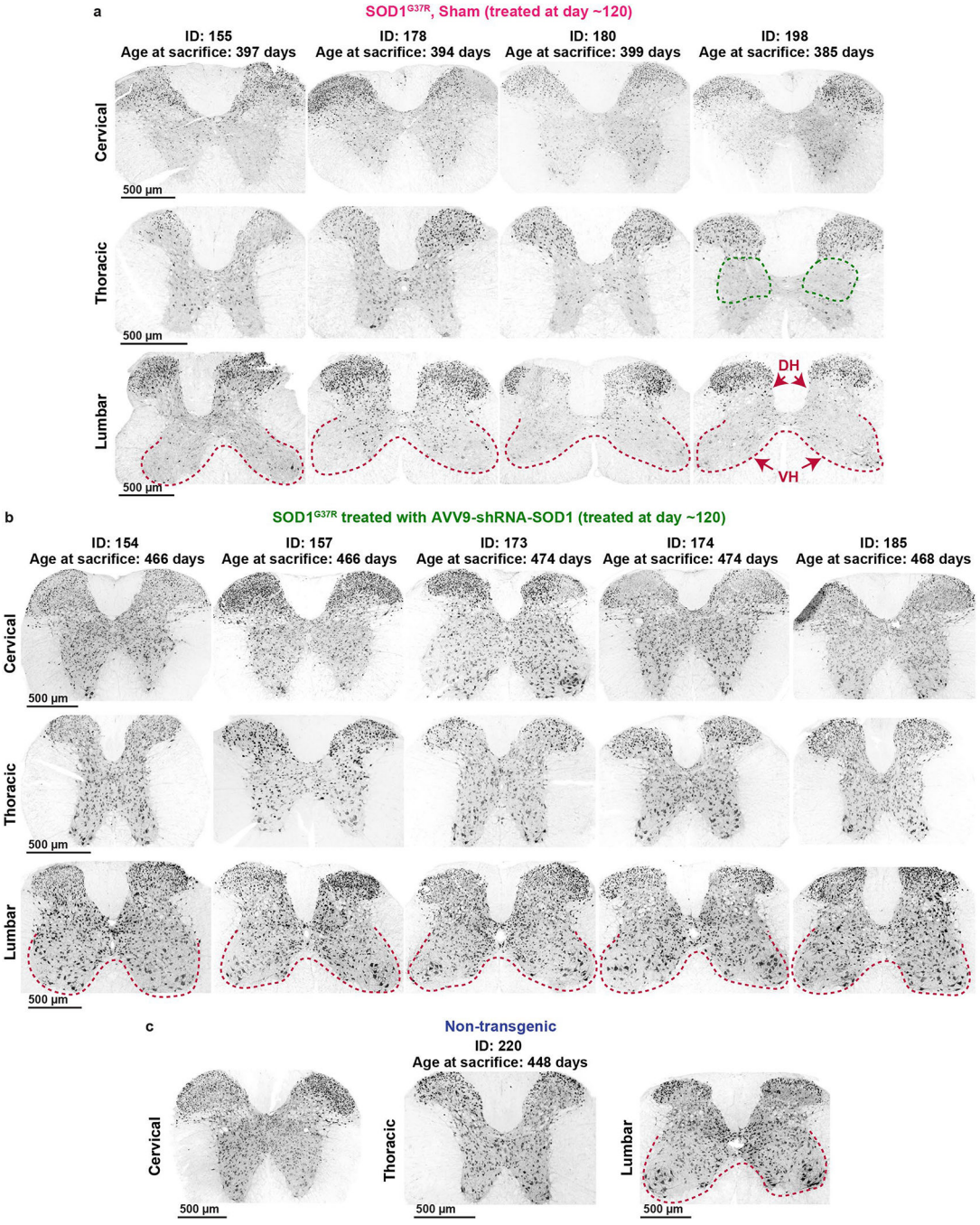

Extended Data Fig. 4 |. Neuronal protection in cervical, thoracic and lumbar spinal cord of *SOD1*^{G37R} mice after pre-symptomatic subpial injection of AAV9-shRNA-*SOD1*.

a,b,c, Transverse spinal cord sections taken from the cervical, thoracic and lumbar spinal cord from four sham-operated *SOD1*^{G37R} animals, five *SOD1*^{G37R} animals subpially-

injected presymptomatically at ~120 days of age with AAV-9-shRNA-*SOD1* and one non-transgenic mouse. Each mouse was analyzed between 394–474 days of age. Neurons were visualized with NeuN antibody. A clear loss of large α-motoneurons in the ventral horn (red dotted area; **a**, lumbar images) was seen in all four sham-operated animals at all segmental levels. NeuN staining intensity was decreased in the intermediate zone (Lamina VII; green dotted area; **a**, thoracic image) throughout the whole spinal cord, while there was complete preservation of α-motoneurons and NeuN staining intensity (similar to wil-type nontransgenic; (**c**)) in Lamina VII of (**b**) all five AAV9-shRNA-*SOD1*-treated $SOD1^{G37R}$ animals in cervical, thoracic and lumbar spinal cord sections.

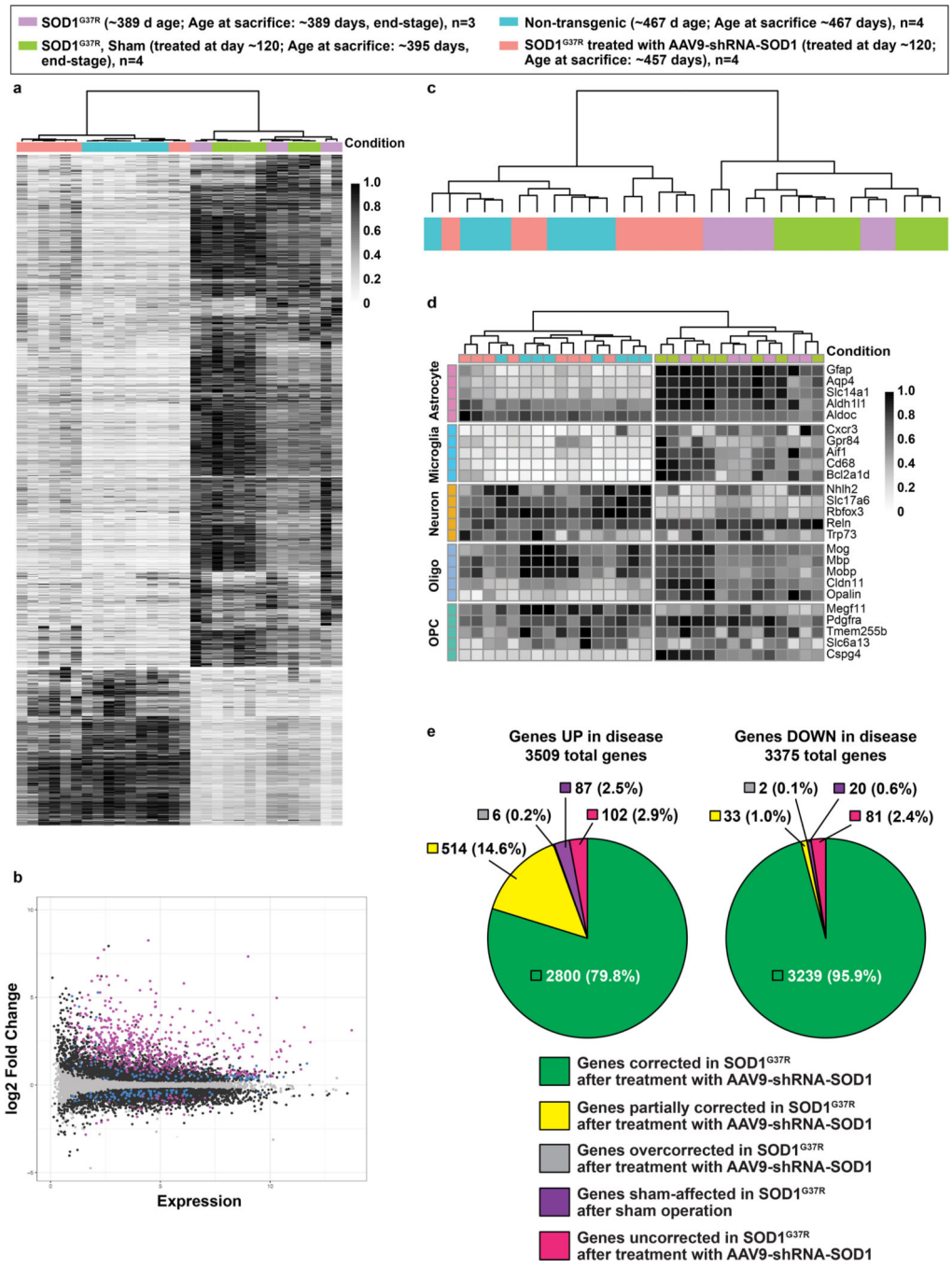

Extended Data Fig. 5 |. Preservation of normal spinal mRNA profile in *SOD1^{G37R}* mice treated subpially before disease onset with AAV9-shRNA-*SOD1*.

a, Heat map showing all genes with greater than two-fold upregulation or downregulation in all experimental groups. Expression is shown on a normalized scale from 0–1. **b**, Scatter plot showing differential gene expression between *SOD1^{G37R}*, sham-operated *SOD1^{G37R}*, wild-type nontransgenic, and *SOD1^{G37R}* AAV9-shRNA-*SOD1*-treated mice. (gray) genes not differentially expressed; (black) genes that were differentially expressed in *SOD1^{G37R}* control (end stage) + sham-operated *SOD1^{G37R}* (end stage) and which expression levels

were corrected in *SOD1*^{G37R} mice after AAV9-shRNA-*SOD1* treatment; (blue) genes still differentially expressed in *SOD1*^{G37R} mice treated with AAV9-shRNA-*SOD1*; (magenta) partially corrected genes that are still differentially expressed in AAV9-shRNA-*SOD1*-treated *SOD1*^{G37R} mice, but partially corrected relative to wild-type nontransgenic mice and either *SOD1*^{G37R} (end stage) or sham-operated *SOD1*^{G37R} (end stage). **c**, Clustering dendrogram demonstrating variation in gene expression across all samples. AAV9-shRNA-*SOD1*-treated *SOD1*^{G37R} samples cluster together with wild-type nontransgenic controls and are very distinct from untreated and sham-operated *SOD1*^{G37R} samples. The primary branch at the top of the dendrogram represents disease/treatment status. **d**, Heat map showing significant upregulation of microglial and astrocytic genes and down regulation of neuronal genes in *SOD1*^{G37R} (end stage) and sham-operated *SOD1*^{G37R} (end stage) mice versus wild-type nontransgenic and AAV9-shRNA-*SOD1*-treated *SOD1*^{G37R}. **e**, Quantification of genes that are differentially expressed in untreated *SOD1*^{G37R} (end stage) and sham-operated *SOD1*^{G37R} (end stage) versus wild-type nontransgenic mice, and the number of genes that are corrected or partially corrected in AAV9-shRNA-*SOD1*-treated *SOD1*^{G37R} mice. Number of animals used (n = number of biologically independent animals) in mRNA sequencing analysis shown above: wild-type nontransgenic (n = 4), untreated *SOD1*^{G37R} end-stage disease (n = 3), sham-treated *SOD1*^{G37R} end-stage disease (n = 4), presymptomatically AAV9-shRNA-*SOD1*-treated *SOD1*^{G37R} (n = 4). Differential expression was performed using edgeR two-sided binomial test with Benjamini & Hochberg post-hoc correction.

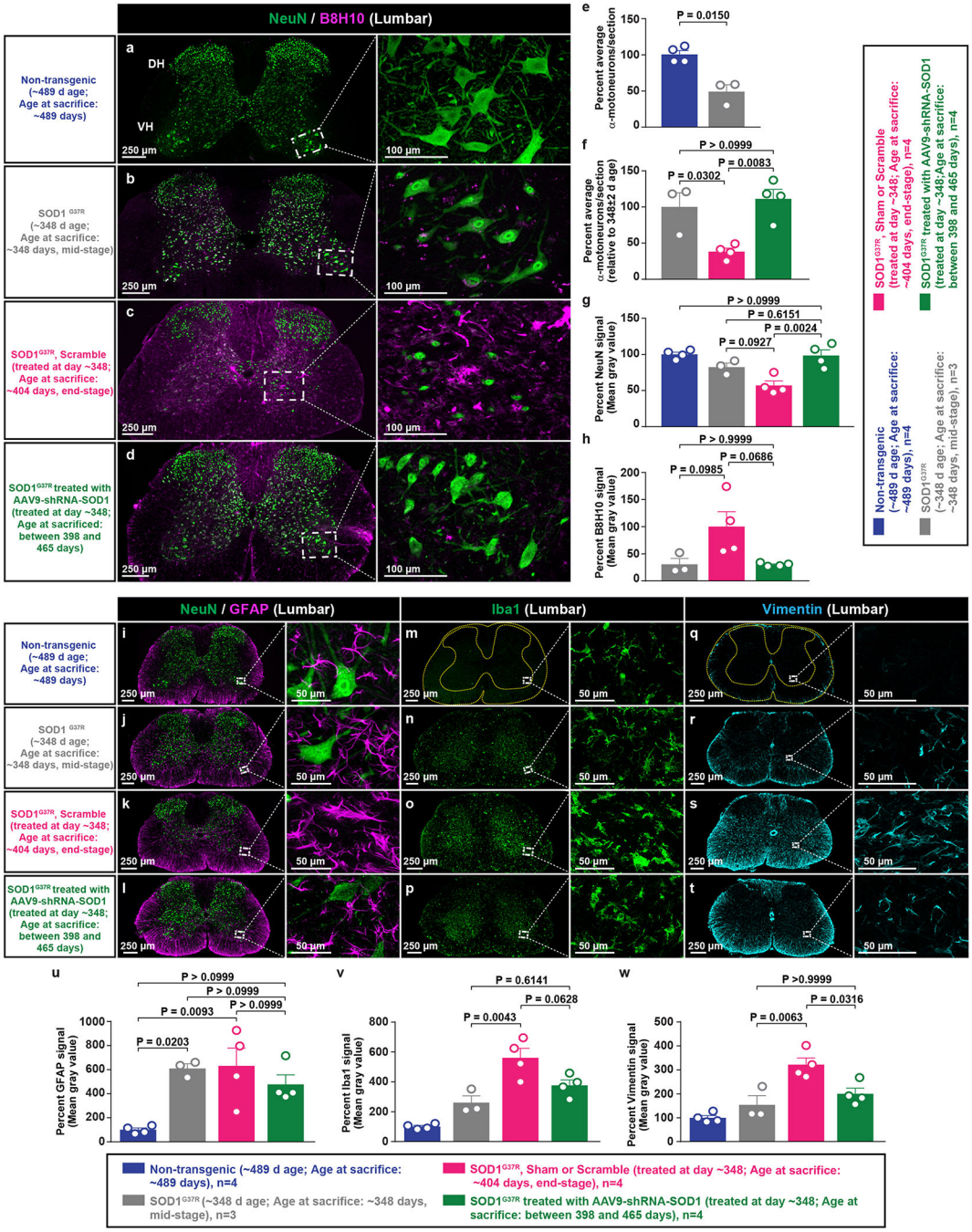

Extended Data Fig. 6 |. Preservation of the remaining lumbar α-motoneurons, interneurons, and suppression of spinal parenchymal misfolded SOD1 in *SOD1^{G37R}* mice treated after disease onset by subpial injection of AAV9-shRNA-*SOD1*.

a-d, Representative transverse lumbar spinal cord sections stained with NeuN (green) and B8H10 (magenta) antibody in mice that were (**a**) 489 ± 6 days old wild-type nontransgenic, (**b**) 348 ± 2 days old *SOD1^{G37R}*, (**c,d**) 404 ± 14 days old, end stage *SOD1^{G37R}* injected subpially with (**c**) AAV9-scrambled virus or (**d**) AAV9-shRNA-*SOD1* and then assayed 90 days later at ages between 398 and 465 days. (**b**) α-motoneurons and early accumulation of aggregates of mutant SOD1 are seen in 348 ± 2 day old *SOD1^{G37R}* mice, while those

neurons and NeuN staining intensity are (**c**) nearly completely lost by end-stage accompanied by marked accumulation of mutant SOD1 in intermediate zone and in ventral horn. **d**, Remaining α-motoneurons in AAV9-shRNA-*SOD1*-treated *SOD1*^{G37R} mice and potent suppression of aggregates of misfolded SOD1 in the ventral horn. **e-h**, Quantitative analysis of α-motoneuron survival, NeuN staining intensity, and misfolded SOD1 protein accumulation. Each dot represents an individual animal; at least 4 sections per animal were used. **i-t**, Representative transverse lumbar spinal cord sections stained with NeuN (green), GFAP (magenta), Iba1 (green) or vimentin (blue) antibodies in (**i**) 348 ± 2 day old wild-type nontransgenic, (**j**) 348 ± 2 day old *SOD1*^{G37R}, and (**k,l**) *SOD1*^{G37R} subpially injected at ~348 days of age with (**k**) AAV9-scrambled virus and harvested at 404 ± 14 days of age (end-stage) or (**l**) AAV9-shRNA-*SOD1* and subsequently aged to 398–465 days (~90 days post-treatment). **u-w**, Quantitation of GFAP, Iba1, and vimentin in each genotype/experimental group. Each dot represents an individual animal; at least 4 sections per animal were used. Experimental animals used: *SOD1*^{G37R} (348 ± 2 days of age, n = 3); Sham-operated (or injected with scramble-AAV9) *SOD1*^{G37R} (n = 4); AAV9-shRNA-*SOD1*-treated *SOD1*^{G37R} (n = 4); and wild-type nontransgenic (n = 4) mice. Data are mean ± S.E.M. Statistical significance was determined with (e) two tail unpaired t-test with Welch's correction ($P = 0.0150$, $t = 4.680$, $df = 3.288$) and with (f-h, u-w) one-way ANOVA followed by Bonferroni post hoc test (**f:** ANOVA, $P = 0.0061$, $F = 10.29$; **g:** ANOVA, $P = 0.0009$, $F = 11.71$; **h:** ANOVA, $P = 0.0394$, $F = 4.980$; **u:** ANOVA, $P = 0.0060$, $F = 7.223$; **v:** ANOVA, $P < 0.0001$, $F = 20.73$; **w:** ANOVA, $P = 0.0004$, $F = 14.30$). P values are shown between the indicated groups. DH, dorsal horn; VH, ventral horn.

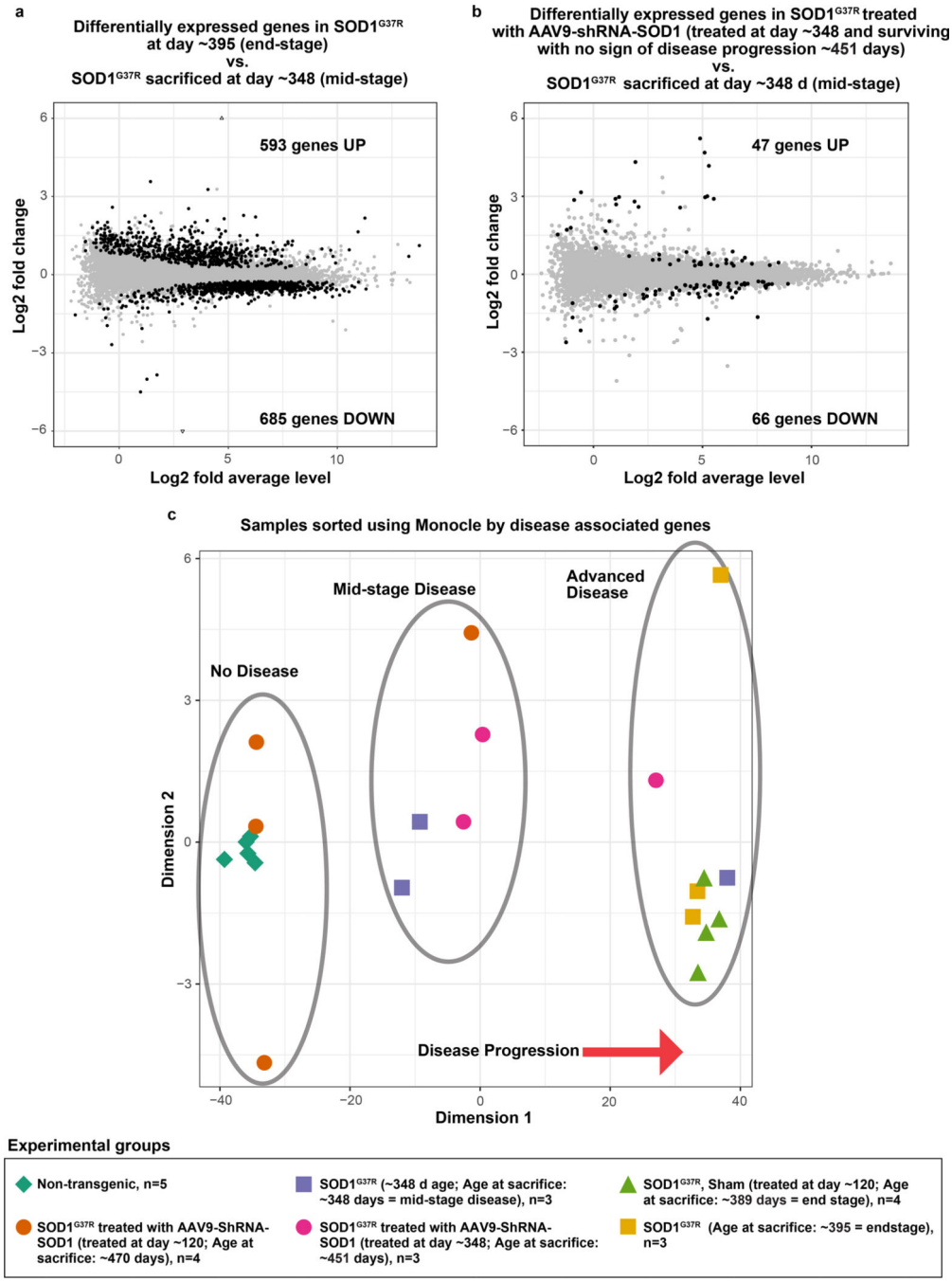

Extended Data Fig. 7 |. Preservation of lumbar spinal cord mRNA profile in *SOD1*^{G37R} mice treated subpially after disease onset with AAV9-shRNA-*SOD1*.

a, Scatter plot showing differentially expressed genes identified (by RNA seq) between non-treated *SOD1*^{G37R} animals analyzed after disease onset (~348 days of age) and untreated end-stage *SOD1*^{G37R} animals (~395 days of age). Compared to comparable analyses from mid-stage disease animals, 593 genes were upregulated and 685 downregulated in end-stage *SOD1*^{G37R} mice. **b**, Scatter plot showing differentially expressed genes between non-treated *SOD1*^{G37R} animals after disease onset (~348 days of age) and *SOD1*^{G37R} animals treated

with AAV9-shRNA-*SOD1* after disease onset (at ~348 days of age) and surviving for additional 96 days with no clinical signs of disease. Only 47 genes were upregulated and 66 downregulated when comparing mid-stage diseased animals to AAV9-shRNA-*SOD1*-treated $SOD1^{G37R}$ mice. Each dot in **a** and **b** represents one gene. Black circles represent genes that are differentially expressed between the two conditions, and gray circles represent genes that are statistically unchanged. Open triangles represent genes that fall outside of the y-axis scale (only two genes fit this category in A). **c**, Minimum spanning tree plots sampled by expression of *SOD1* disease-associated genes generated using DDRTree dimension reduction in Monocle. Data from all experimental groups are presented. Wild-type nontransgenic mice and $SOD1^{G37R}$ mice treated with AAV9-shRNA-*SOD1* before disease onset (at age~120 days) cluster to the left; mid-stage disease $SOD1^{G37R}$, non-treated and $SOD1^{G37R}$ treated at mid-stage disease (at age ~348 days) and then surviving for additional 96 days cluster in the middle. All non-treated end-stage (end stage disease) $SOD1^{G37R}$ animals cluster at the right. Number of animals used (n = number of biologically independent animals) in mRNA sequencing analysis shown above: wild-type nontransgenic (n = 5), untreated $SOD1^{G37R}$ end-stage disease (n = 3), sham-treated $SOD1^{G37R}$ end-stage disease (n = 4), presymptomatic AAV9-shRNA-*SOD1*-treated $SOD1^{G37R}$ (n = 4), untreated $SOD1^{G37R}$ mid-stage disease (n = 3), postsymptomatic AAV9-shRNA-*SOD1*-treated $SOD1^{G37R}$ (n = 3). Differential expression was performed using edgeR two-sided binomial test with Benjamini & Hochberg post-hoc correction.

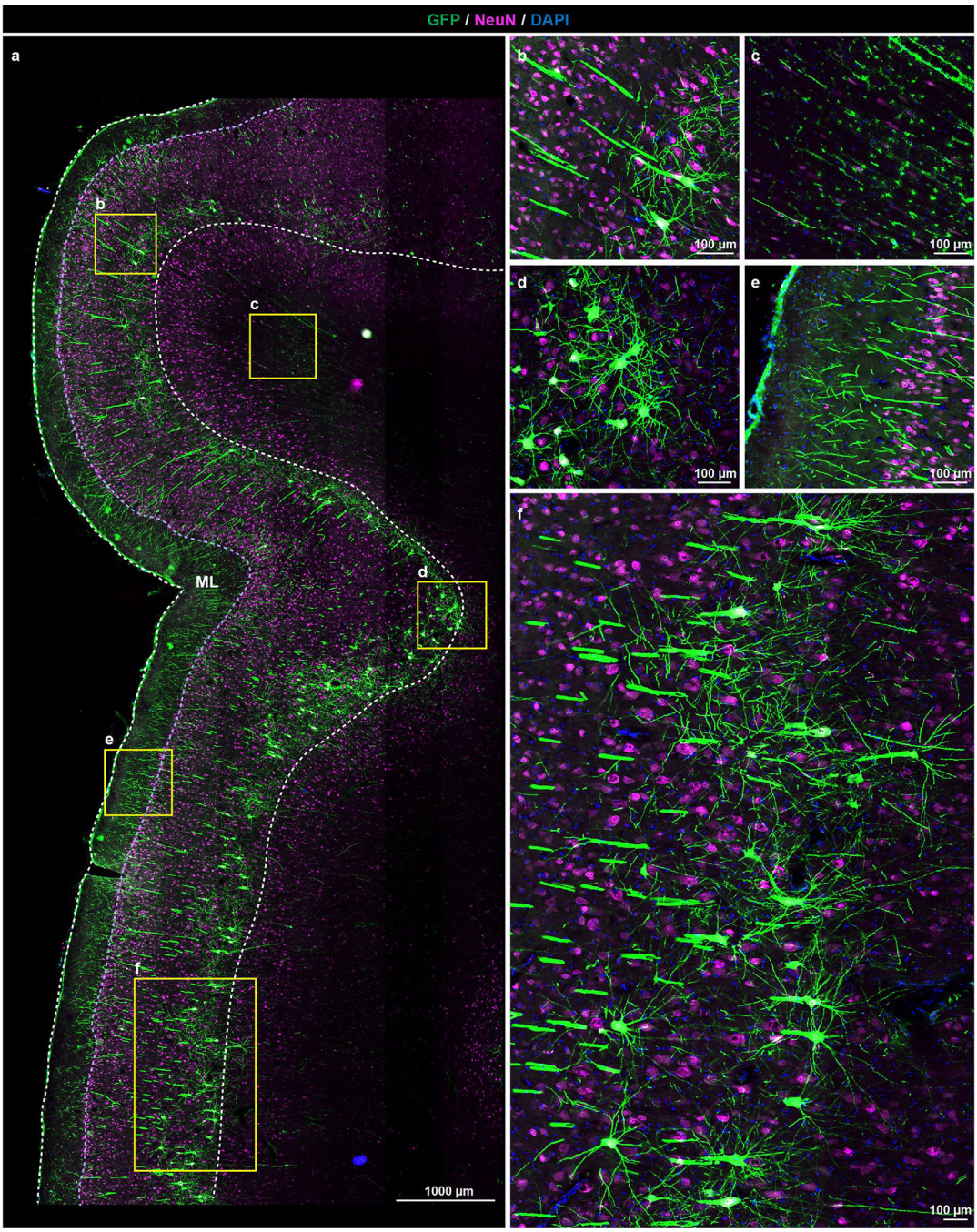

Extended Data Fig. 8 |. Widespread GFP expression in pyramidal neurons of motor cortex after a single bolus cervical subpial delivery of AAV9-UBI-*GFP* in adult pig.

a-f, Intense GFP expression throughout the majority of pyramidal neuron population in layer V of the motor cortex at 3 weeks after a single bolus cervical subpial delivery of AAV9-UBI-*GFP* in an adult pig. GFP expression was not detected in glial cells localized in the molecular layer, consistent with retrograde AAV delivery to pyramidal neurons from corticospinal axons transiting through or terminating in subpially-injected cervical spinal cord segments. A representative result of 3 individual pigs is shown. ML, molecular layer.

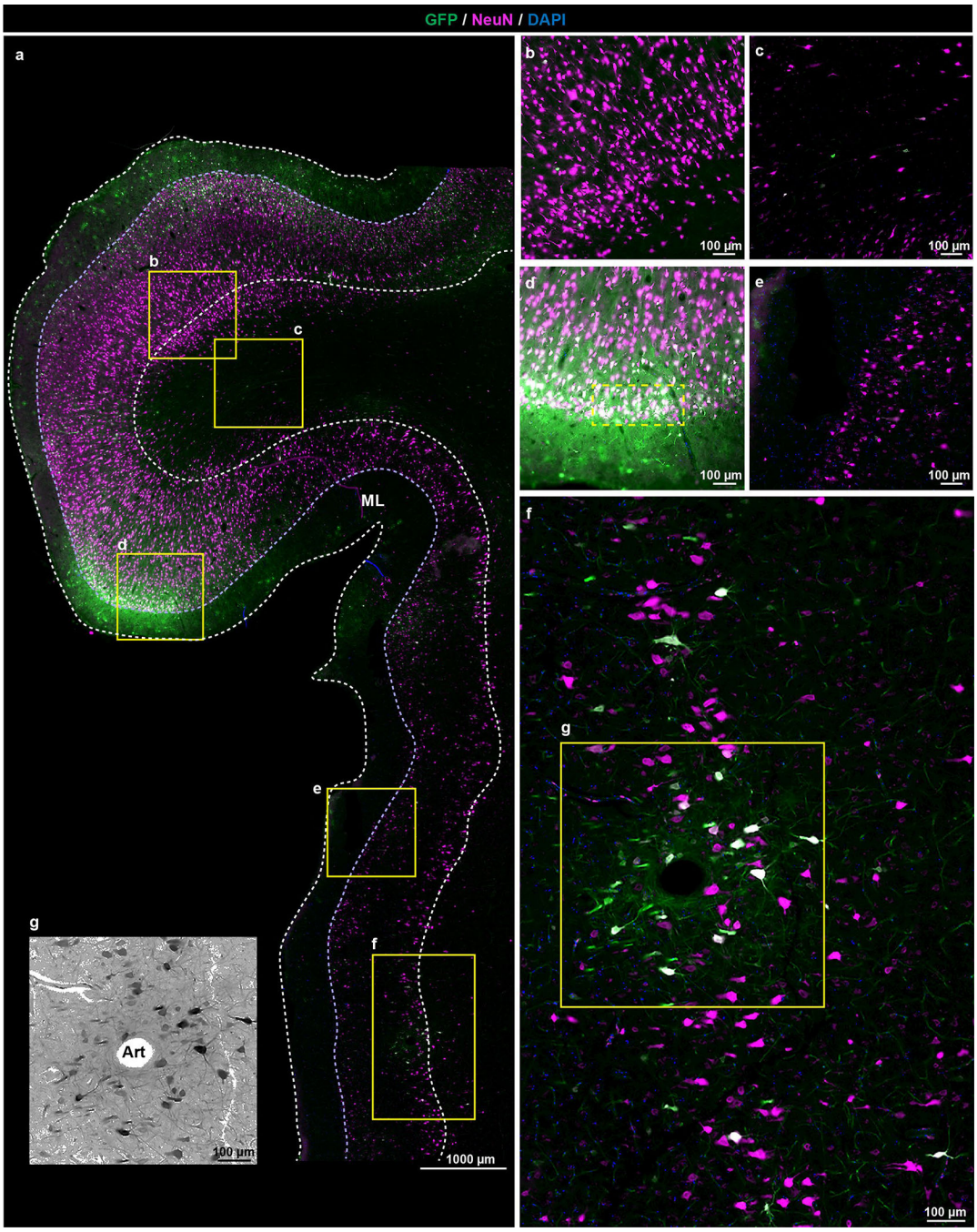

Extended Data Fig. 9 |. Limited GFP expression in motor cortex neurons after single intrathecal bolus cervical delivery of AAV9-UBI-*GFP* to adult pig.

a-e, Irregularly distributed GFP+ immunoreactive regions in the cortical molecular layer, with GFP+ neurons in layer II-III (**d**, white-boxed area) 21 days following single intrathecal bolus cervical delivery of AAV9-UBI-*GFP* in an adult pig. **f, g**, GFP+ non-pyramidal neurons identified in deeper cortical layers, primarily found in the vicinity of cerebral arteries, suggesting perivascular AAV9 diffusion into brain parenchyma. A representative result of 3 individual pigs is shown. Art, arterial lumen.

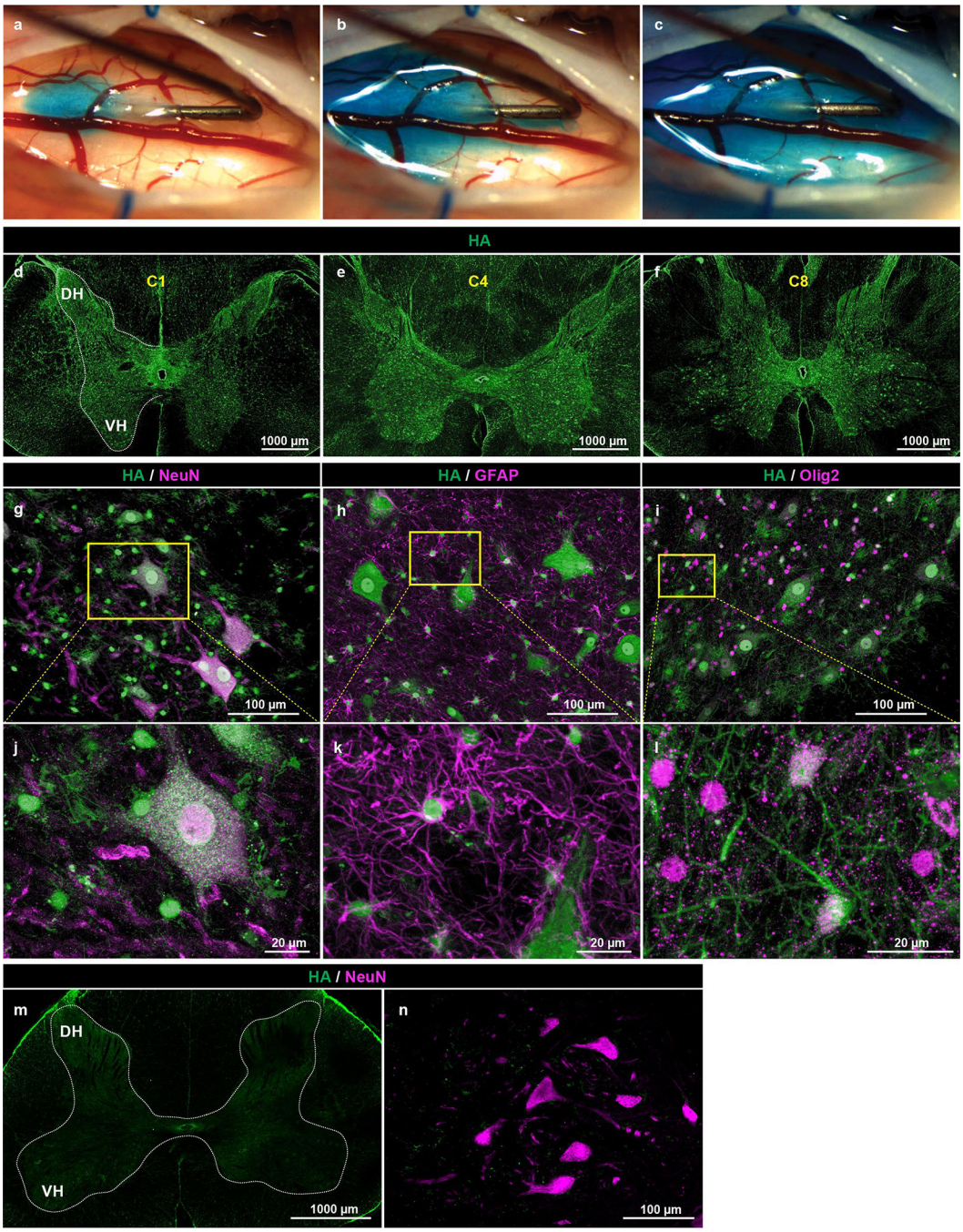

Extended Data Fig. 10 |. Effective AAV9-encoded gene expression throughout the entire cervical spinal cord of the adult monkey after a single bolus, subpial C3 delivery of AAV9-UBI-*Rpl22*-3×*HA*.

a-c, An intraoperative photograph depicting the placement of subpial injection needle in the C3-C4 segment and rostro-caudal spread of 'blue' dextran (10,000 MW; 300 µl) immediately after initiation of subpial infusion (1 µl/5 sec). **d-f**, Expression of Rpl22 protein (anti-HA staining; green signal) in cervical spinal cord segments (C1-C8) at 48 h after mid-cervical subpial AAV9-UBI-*Rpl22*-3x*HA* delivery. **g-l**, Neuronal (NeuN), astrocyte (GFAP) and oligodendrocyte (Olig2)-expression of Rpl22 protein (HA+ signal) at 48 h after AAV9-

UBI-*Rpl22*-3x*HA* delivery. **m, n**, Absence of specific staining in non-injected animals. A representative result of 2 individual non-human primates per group is shown (Subpially-injected, n = 2; Control non-injected, n = 2). DH, dorsal horn; VH, ventral horn.

Supplementary Material

Refer to Web version on PubMed Central for supplementary material.

Acknowledgements

H. Skalnikova, S.J. and J.J. are supported by the National Sustainability Program I, of the Czech Ministry of Education, Youth and Sports (no. LO1609) and RVO (no. 67985904). Z.T. is supported by the Slovak Research and Development Agency (APVV-15–0665) and by the Scientific Grant Agency of the Ministry of Education, Science, Research and Sport of the Slovak Republic and the Slovak Academy of Sciences (VEGA 2/0086/16). I.V. is supported by the Slovak Research and Development Agency (APVV 14–0847). H. Studenovska and V.P. are supported by the Czech Science Foundation (project no. 18–04393S). E.T.A is supported by the NIH (grant no. R01-EB024015) and the California Institute for Regenerative Medicine (grant no. LA1-C12–06919). B.K.K, D.W.C. and M.M. are supported by the ALS Association and Sanford Porcine Center.

References

1. Rosen DR et al. Mutations in Cu/Zn superoxide dismutase gene are associated with familial amyotrophic lateral sclerosis. Nature 362, 59–62 (1993). [PubMed: 8446170]
2. Matsumoto A et al. Disease progression of human SOD1 (G93A) transgenic ALS model rats. J. Neurosci. Res. 83, 119–133 (2006). [PubMed: 16342121]
3. Kaur SJ, McKeown SR & Rashid S Mutant SOD1 mediated pathogenesis of amyotrophic lateral sclerosis. Gene 577, 109–118 (2016). [PubMed: 26657039]
4. van Zundert B & Brown RH Jr. Silencing strategies for therapy of SOD1-mediated ALS. Neurosci. Lett. 636, 32–39 (2017). [PubMed: 27507699]
5. Howland DS et al. Focal loss of the glutamate transporter EAAT2 in a transgenic rat model of SOD1 mutant-mediated amyotrophic lateral sclerosis (ALS). Proc. Natl Acad. Sci. USA 99, 1604–1609 (2002). [PubMed: 11818550]
6. McGoldrick P, Joyce PI, Fisher EM & Greensmith L Rodent models of amyotrophic lateral sclerosis. Biochim. Biophys. Acta. 1832, 1421–1436 (2013). [PubMed: 23524377]
7. Ilieva H, Polymenidou M & Cleveland DW Non-cell autonomous toxicity in neurodegenerative disorders: ALS and beyond. J. Cell Biol. 187, 761–772 (2009). [PubMed: 19951898]
8. Yamanaka K et al. Mutant SOD1 in cell types other than motor neurons and oligodendrocytes accelerates onset of disease in ALS mice. Proc. Natl Acad. Sci. USA 105, 7594–7599 (2008). [PubMed: 18492803]
9. Kang SH et al. Degeneration and impaired regeneration of gray matter oligodendrocytes in amyotrophic lateral sclerosis. Nat. Neurosci. 16, 571–579 (2013). [PubMed: 23542689]
10. Hefferan MP et al. Human neural stem cell replacement therapy for amyotrophic lateral sclerosis by spinal transplantation. PLoS ONE 7, e42614 (2012). [PubMed: 22916141]
11. Boillee S et al. Onset and progression in inherited ALS determined by motor neurons and microglia. Science 312, 1389–1392 (2006). [PubMed: 16741123]
12. Yamanaka K et al. Astrocytes as determinants of disease progression in inherited amyotrophic lateral sclerosis. Nat. Neurosci. 11, 251–253 (2008). [PubMed: 18246065]
13. Borel F et al. Therapeutic rAAVrh10 mediated SOD1 silencing in adult SOD1(G93A) mice and nonhuman primates. Hum. Gene Ther. 27, 19–31 (2016). [PubMed: 26710998]
14. Iannitti T et al. Translating SOD1 gene silencing toward the clinic: a highly efficacious, off-target-free, and biomarker-supported strategy for fALS. Mol. Ther. Nucleic Acids 12, 75–88 (2018). [PubMed: 30195799]

15. Stoica L et al. Adeno-associated virus-delivered artificial microRNA extends survival and delays paralysis in an amyotrophic lateral sclerosis mouse model. Ann. Neurol. 79, 687–700 (2016). [PubMed: 26891182]
16. Foust KD et al. Therapeutic AAV9-mediated suppression of mutant SOD1 slows disease progression and extends survival in models of inherited ALS. Mol. Ther. 21, 2148–2159 (2013). [PubMed: 24008656]
17. Smith RA et al. Antisense oligonucleotide therapy for neurodegenerative disease. J. Clin. Invest. 116, 2290–2296 (2006). [PubMed: 16878173]
18. McCampbell A et al. Antisense oligonucleotides extend survival and reverse decrement in muscle response in ALS models. J. Clin. Invest. 128, 3558–3567 (2018). [PubMed: 30010620]
19. Biferi MG et al. A new AAV10-U7-mediated gene therapy prolongs survival and restores function in an ALS mouse model. Mol. Ther. 25, 2038–2052 (2017). [PubMed: 28663100]
20. Miyanohara A et al. Potent spinal parenchymal AAV9-mediated gene delivery by subpial injection in adult rats and pigs. Mol. Ther. Methods Clin. Dev. 3, 16046 (2016). [PubMed: 27462649]
21. Tadokoro T et al. Subpial adeno-associated virus 9 (AAV9) vector delivery in adult mice. J. Vis. Exp. 125, 55770 (2017).
22. Wong PC et al. An adverse property of a familial ALS-linked SOD1 mutation causes motor neuron disease characterized by vacuolar degeneration of mitochondria. Neuron 14, 1105–1116 (1995). [PubMed: 7605627]
23. Parone PA et al. Enhancing mitochondrial calcium buffering capacity reduces aggregation of misfolded SOD1 and motor neuron cell death without extending survival in mouse models of inherited amyotrophic lateral sclerosis. J. Neurosci. 33, 4657–4671 (2013). [PubMed: 23486940]
24. Filali M, Lalonde R & Rivest S Sensorimotor and cognitive functions in a $SOD1^{G37R}$ transgenic mouse model of amyotrophic lateral sclerosis. Behav. Brain Res. 225, 215–221 (2011). [PubMed: 21816178]
25. Gros-Louis F, Soucy G, Lariviere R & Julien JP Intracerebroventricular infusion of monoclonal antibody or its derived Fab fragment against misfolded forms of SOD1 mutant delays mortality in a mouse model of ALS. J. Neurochem. 113, 1188–1199 (2010). [PubMed: 20345765]
26. Tanaka Y et al. Cardiac sympathetic function in the patients with amyotrophic lateral sclerosis: analysis using cardiac [123I]MIBG scintigraphy. J. Neurol. 260, 2380–2386 (2013). [PubMed: 23784610]
27. Linden D, Diehl RR & Berlit P Reduced baroreflex sensitivity and cardiorespiratory transfer in amyotrophic lateral sclerosis. Electroencephalogr. Clin. Neurophysiol. 109, 387–390 (1998). [PubMed: 9851294]
28. Dalla Vecchia L et al. Cardiovascular neural regulation is impaired in amyotrophic lateral sclerosis patients. A study by spectral and complexity analysis of cardiovascular oscillations. Physiol. Meas. 36, 659–670 (2015). [PubMed: 25798998]
29. Chapleau MW & Sabharwal R Methods of assessing vagus nerve activity and reflexes. Heart Fail. Rev. 16, 109–127 (2011). [PubMed: 20577901]
30. Caravaca AS et al. A novel flexible cuff-like microelectrode for dual purpose, acute and chronic electrical interfacing with the mouse cervical vagus nerve. J. Neural Eng. 14, 066005 (2017). [PubMed: 28628030]
31. Shimizu T, Kato S, Hayashi M, Hayashi H & Tanabe H Amyotrophic lateral sclerosis with hypertensive attacks: blood pressure changes in response to drug administration. Clin. Auton. Res. 6, 241–244 (1996). [PubMed: 8902322]
32. Shemisa K, Kaelber D, Parikh SA & Mackall JA Autonomic etiology of heart block in amyotrophic lateral sclerosis: a case report. J. Med. Case Rep. 8, 224 (2014). [PubMed: 24961916]
33. Usvald D et al. Analysis of dosing regimen and reproducibility of intraspinal grafting of human spinal stem cells in immunosuppressed minipigs. Cell Transplant. 19, 1103–1122 (2010). [PubMed: 20412634]
34. Federici T, Riley J, Park J, Bain M & Boulis N Preclinical safety validation of a stabilized viral vector direct injection approach to the cervical spinal cord. Clin. Transl. Sci. 2, 165–167 (2009). [PubMed: 20443884]

35. Xiao X, Li J & Samulski RJ Production of high-titer recombinant adeno-associated virus vectors in the absence of helper adenovirus. J. Virol. 72, 2224–2232 (1998). [PubMed: 9499080]

36. Lai NC et al. Improved function of the failing rat heart by regulated expression of insulin-like growth factor I via intramuscular gene transfer. Hum. Gene Ther. 23, 255–261 (2012). [PubMed: 22017392]

37. Xu Q et al. In vivo gene knockdown in rat dorsal root ganglia mediated by self-complementary adeno-associated virus serotype 5 following intrathecal delivery. PLoS ONE 7, e32581 (2012). [PubMed: 22403675]

38. Herzog A & Brosamle C 'Semifree-floating' treatment: a simple and fast method to process consecutive sections for immunohistochemistry and neuronal tracing. J. Neurosci. Methods 72, 57–63 (1997). [PubMed: 9128169]

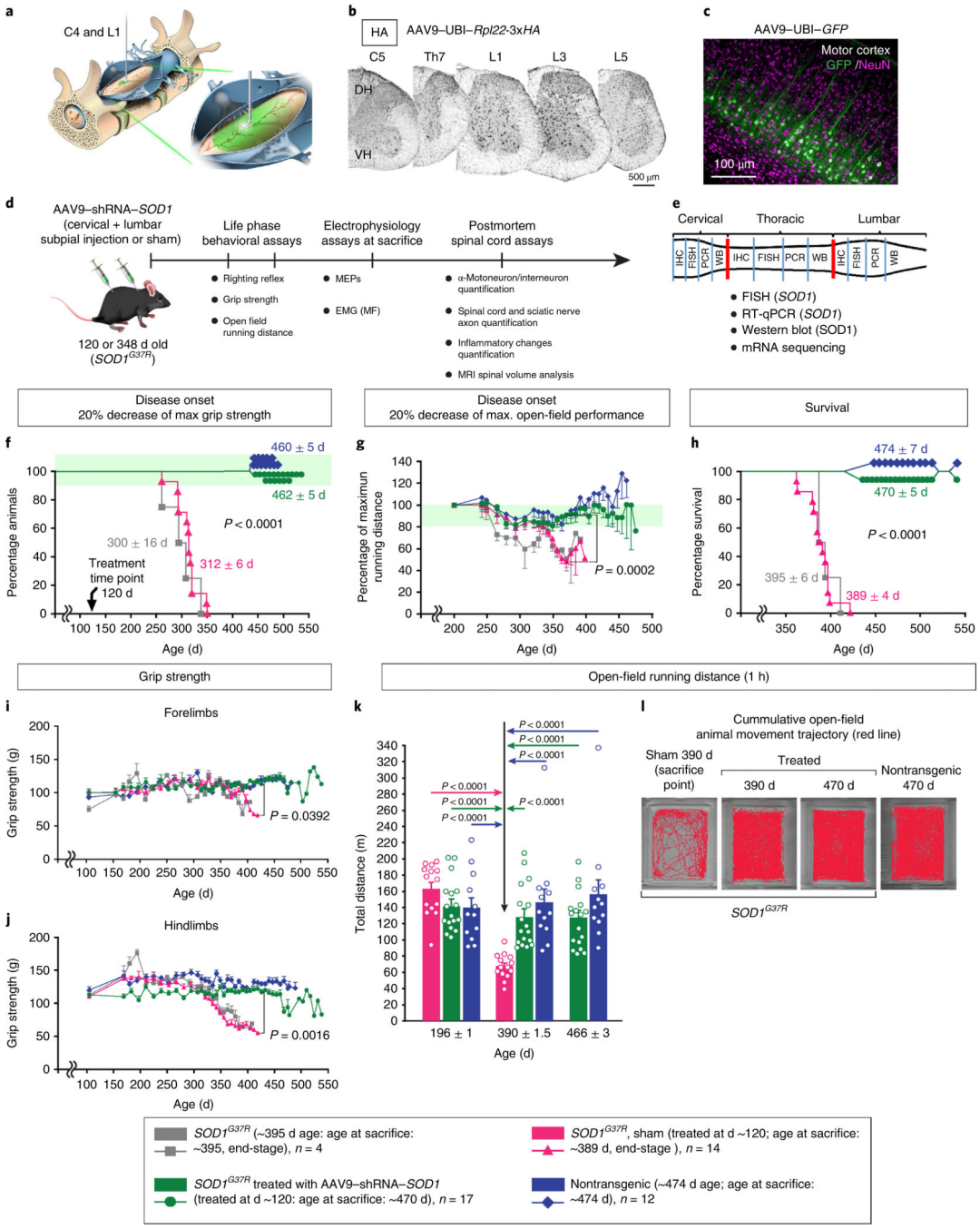

Fig. 1 |. Spinal SP AAV9–shRNA–*SOD1* delivery before disease onset in *SOD1*^{G37R} mice blocks disease onset, producing long-term preservation of motor function.

a, Schematic of upper cervical and lumbar SP delivery of AAV9. **b**,**c** Widespread AAV9 delivery and expression of an AAV9-encoded gene in the dorsal and ventral horns of adult mice, identified by immunohistochemistry of spinal cord sections taken from different segmental levels (**b**) or immunofluorescence of motor cortex (**c**) after a single upper cervical and lumbar SP delivery of AAV9–*Rpl22*-x3*HA* (**b**) (imaged 48 h after AAV9 injection) or AAV9–UBI–*GFP* (**c**) (imaged 14 d after AAV9 injection), retrogradely delivered to the

motor cortex. A representative result from four independent mice is shown. **d**,**e**, Schematic diagrams of the experimental design and 'in-life' and 'postmortem' assays. **f**,**g**, Disease onset (defined as 20% decrease of maximum grip strength (**f**) or 20% decrease of maximum open-field performance (**g**)). **h**, Survival (measured by normal righting reflex) in $SOD1^{G37R}$ mice with or without SP AAV9–shRNA–*SOD1* injection before disease onset. **i**,**j**, Grip strength in forelimbs (**i**) and hindlimbs (**j**) with and without AAV9–shRNA–*SOD1* treatment. **k**,**l**, Open-field motor performance (running distance per 1 h) with and without SP AAV9–shRNA–*SOD1* treatment. Data are expressed as mean ± s.e.m. (squares: nontreated $SOD1^{G37R}$ mice ($n = 4$); triangle: sham-operated $SOD1^{G37R}$ mice ($n = 14$); circles: shRNA–*SOD1*-treated $SOD1^{G37R}$ mice ($n = 17$); diamond: normal wild-type mice ($n = 12$)). The statistical significance was determined as follows: Kaplan–Meier survival analysis using the two-sided log-rank test (**f**,**h**); two-way ANOVA followed by Bonferroni's posthoc test (**g**: ANOVA $P_{int} = 0.8737$, $F = 0.7800$; **i**, ANOVA, $P_{int} < 0.0001$, $F = 1.763$; **j**: ANOVA $P_{int} < 0.0001$, $F = 3.50$); **k**, Kruskal–Wallis test followed by Steel–Dwass posthoc test ($P < 0.0001$). *P* values are shown between the indicated groups/time points. DH, dorsal horn; VH, ventral horn.

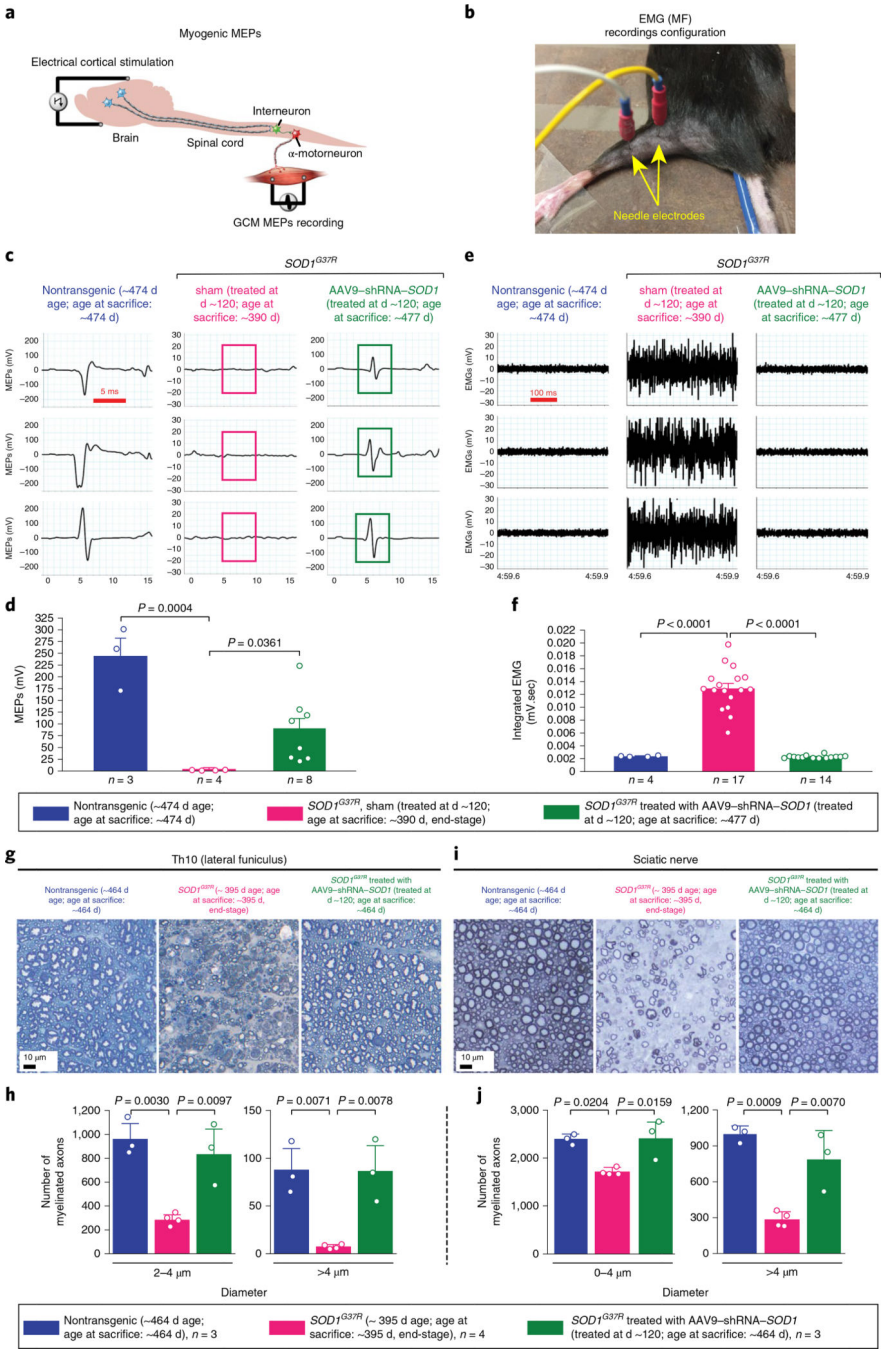

Fig. 2 |. Continuing presence of myogenic MEPs and lack of MF in *SOD1*^{G37R} mice treated before disease onset with AAV9–shRNA–*SOD1*.

a,**b**, Schematics of MEPs (**a**) and EMG (muscle fibrillation: MF) (**b**) recordings. **c**,**d**, Representative MEP recordings from three individual wild-type nontransgenic (left), shamo-perated *SOD1*^{G37R} (middle) and AAV9–shRNA–*SOD1*-treated *SOD1*^{G37R} mice (right). A complete loss of MEP response is seen in sham-operated *SOD1*^{G37R} mice (**c**, middle panel boxes), whereas AAV9–shRNA–*SOD1*-treated *SOD1*^{G37R} mice showed continued MEPs (**c**, right panel boxes), with notable preservation of amplitude (**d**). **e**,**f**, Representative MF

recordings from three wild-type nontransgenic mice (left), sham-operated *SOD1*^{G37R} mice (middle) and AAV9–shRNA-treated *SOD1*^{G37R} mice (right) mice. **g–j**, Microphotographs and axonal quantification of lateral funiculi (Th10) (**g**,**h**) or sciatic nerves (**i**,**j**) of wild-type nontransgenic, untreated *SOD1*^{G37R} or AAV9–shRNA–*SOD1*-treated *SOD1*^{G37R} mice. Data for MEPs (**d**) and MF (**f**) are expressed as mean ± s.e.m.; each dot represents an individual animal. One-way ANOVA was used for statistical analyses (**d**: wild-type nontransgenic mice, $n = 3$; sham-operated *SOD1*^{G37R} mice, $n = 4$; shRNA–*SOD1*-treated *SODG37R* mice, $n = 8$; $P = 0.0007$, $F = 14.09$ using the Holm–Sidak posthoc test; **f**: wild-type nontransgenic mice, $n = 4$; sham-operated *SOD1*^{G37R} mice, $n = 17$; shRNA–*SOD1*-treated *SODG37R* mice, $n = 14$; $P < 0.0001$, $F = 90.55$ using the Holm–Sidak posthoc test). Data on axonal counts (**h**,**j**) are expressed as mean ± s.e.m. (wild-type nontransgenic mice, $n = 3$; *SOD1*^{G37R} nontreated mice, $n = 4$; shRNA–*SOD1*-treated *SODG37R* mice, $n = 3$). The statistical significance was determined using one-way ANOVA followed by Bonferroni's posthoc test (**h**, 2–4 μm: ANOVA, $P = 0.0020$, $F = 17.19$, **h**, >4 μm: ANOVA $P = 0.0030$, $F = 14.83$; **j**, 0–4 μm: ANOVA,$P = 0.0076$, $F = 10.60$, **j**, >4 μm: ANOVA $P = 0.0007$, $F = 23.98$). The P values are shown between the indicated groups.

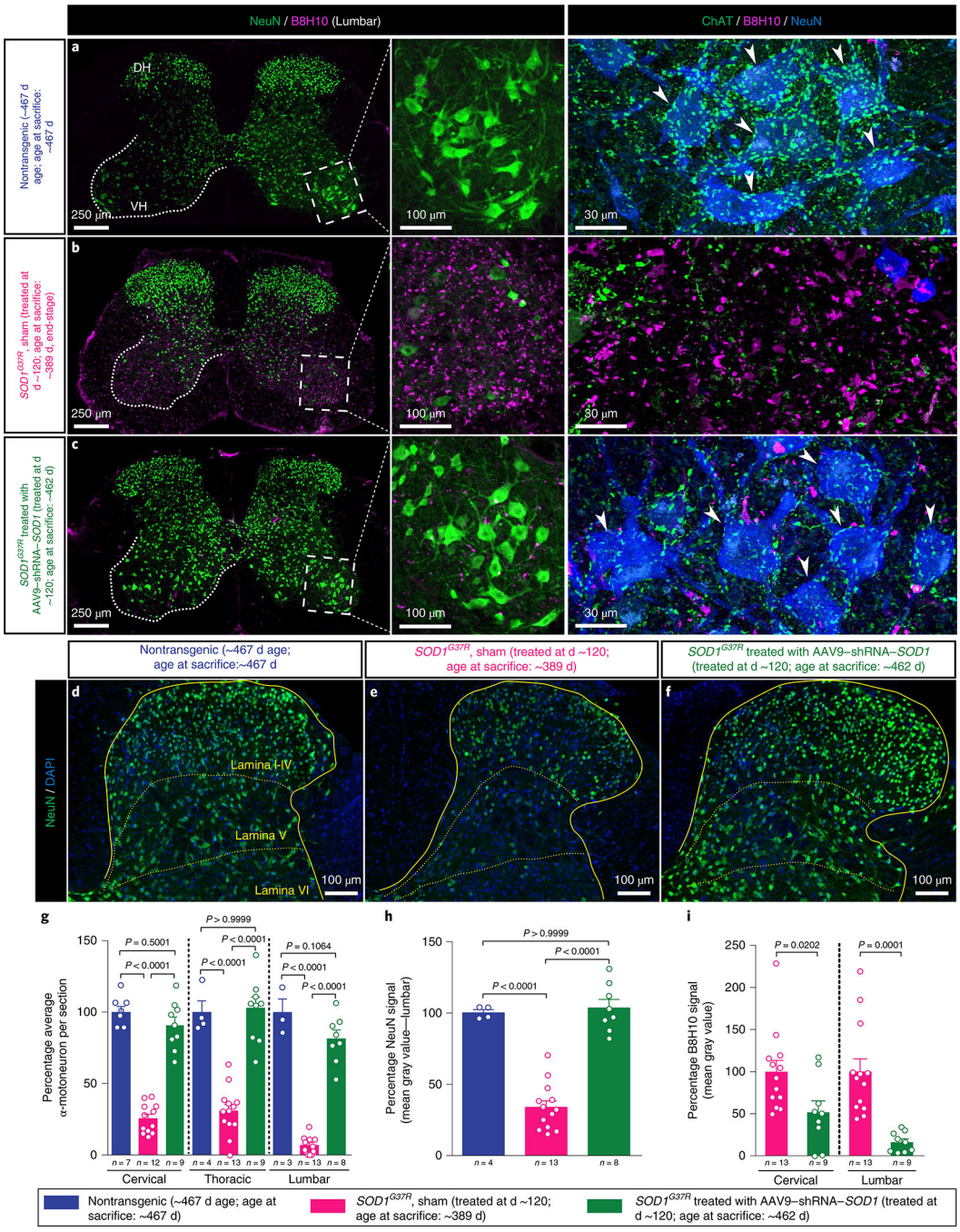

Fig. 3 |. Preservation of spinal α-motoneurons and interneurons, and suppression of misfolded SOD1 protein accumulation in spinal parenchyma of AAV9–shRNA–*SOD1*-treated *SOD1*^{G37R} mice treated before disease onset.

a–c, NeuN, misfolded SOD1 (identified by the B8H10 antibody25) or choline acetyltransferase in lumbar spinal cord sections of wild-type nontransgenic mice (**a**) or *SOD1*^{G37R} mice without (**b**) or with (**c**) SP treatment with AAV9–shRNA–*SOD1* before disease onset. A representative result of at least 12 individual sham-operated *SOD1*^{G37R} mice, 8 individual AAV9–shRNA–*SOD1*-treated *SOD1*^{G37R} mice and 3 individual wild-type nontransgenic mice is shown. **d–f**, Loss of lumbar interneurons expressing NeuN between

laminae IV and VII in sham-operated *SOD1*^{G37R} mice (**e**) relative to wild-type nontransgenic (**d**) but not after treatment with AAV9–shRNA–*SOD1* (**f**) before disease onset. A representative result of 13 individual sham-operated *SOD1*^{G37R} mice, 8 AAV9–shRNA–*SOD1*-treated *SOD1*^{G37R}mice and 4 wild-type nontransgenic mice is shown. **g**–**i**, Quantitative analysis of cervical, thoracic and lumbar α-motoneurons, NeuN expression (lumbar spinal cord) and accumulation of misfolded SOD1 in the cervical and lumbar spinal cord of wild-type nontransgenic, AAV9–shRNA–*SOD1*-treated *SOD1*^{G37R} and untreated *SOD1*^{G37R} mice using at least four sections per animal. All data are expressed as mean ± s.e.m. Each circle represents an individual mouse. Sham-operated *SOD1*^{G37R} mice ($n \geq 12$), AAV9–shRNA–*SOD1*-treated *SOD1*^{G37R} mice ($n \geq 8$) and wild-type nontransgenic mice ($n \geq 3$); the exact individual sample sizes are shown in the corresponding graph. One-way ANOVA followed by Bonferroni's posthoc test was used for statistical analysis in **g** and **h** (**g**, cervical: ANOVA $P < 0.0001$, $F = 100.6$, **g**, thoracic: ANOVA $P < 0.0001$, $F = 47.69$; **g**, lumbar: ANOVA $P < 0.0001$, $F = 134.5$; **h**, ANOVA $P < 0.0001$, $F = 62.16$). The unpaired, two-tailed, Student's *t*-test with Welch's correction was used in **i** (**i**, cervical: $P = 0.0202$, $t = 2.534$, degrees of freedom (d.f.) = 19.04; **i**, lumbar: $P = 0.0001$, $t = 5.354$, d.f. = 13.63.) *P* values are shown between the indicated groups, DH, dorsal horn; VH, ventral horn.

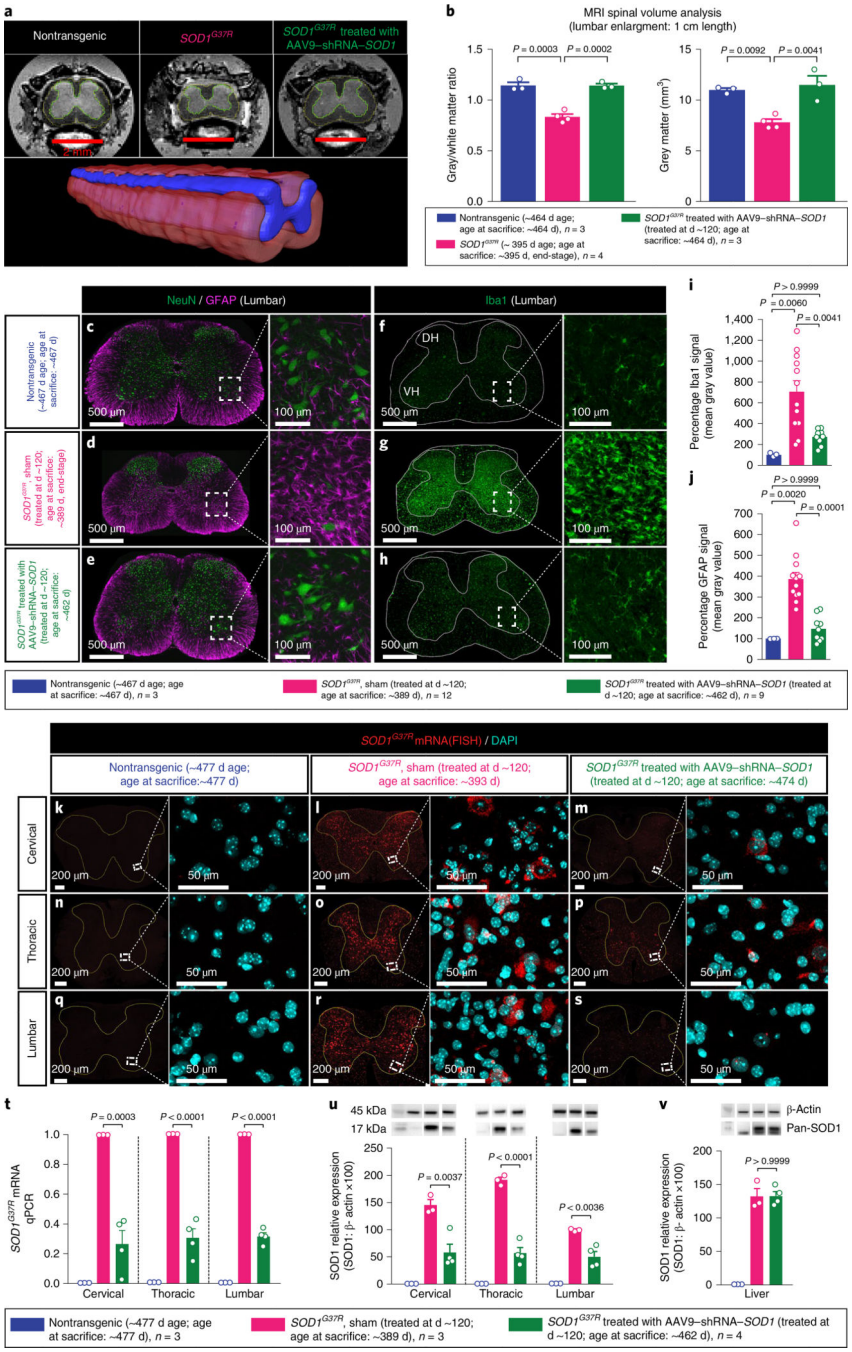

Fig. 4 |. Blockage of spinal cord atrophy and suppression of inflammatory changes and mutant *SOD1* mRNA and protein accumulation in *SOD1*^{G37R} mice treated before disease onset with AAV9–shRNA–*SOD1*.

a,**b**, Notable preservation of the gray matter volume and the gray:white matter ratio determined by MRI-based volumetric analysis of lumbar enlargement in *SOD1*^{G37R} mice treated before disease onset with AAV9–shRNA–*SOD1*. Representative images (**a**) and the result of quantification and statistical analysis (**b**) are shown. Each dot represents an individual animal. **c**–**h**, Suppression of astrocyte activation (marked by GFAP) (**c**–**e**) and microglial activation (marked by Iba1) (**f**–**h**) in *SOD1*^{G37R} mice treated before disease onset

with AAV9–shRNA–*SOD1*, relative to areas of α-motoneuronal loss and decreased NeuN+ staining in the intermediate zone, identified in transverse lumbar sections in sham-operated $SOD1^{G37R}$ mice. **i**,**j**, Quantification by densitometry of Iba 1 (**i**) and GFAP (**j**) reactivity in gray matter of wild-type nontransgenic and treated and untreated $SOD1^{G37R}$ mice, using at least four sections per animal. A representative typical image for each group is shown; each dot represents an individual animal. **k**–**s**, Mutant *SOD1* RNA levels (measured with FISH) in cervical, thoracic and lumbar sections from wild-type nontransgenic (**k**,**n**,**q**), sham-operated $SOD1^{G37R}$ (**l**,**o**,**r**) and $SOD1^{G37R}$ (**m**,**p**,**s**) animals treated before disease onset with AAV9–shRNA–*SOD1*. A representative image of each segment for at least three animals from each group is shown. **t**–**v**, Analysis of mutant *SOD1* RNA or protein levels by qPCR (**t**) or immunoblot (**u**,**v**) of cervical, thoracic and lumbar spinal cord and liver tissue from each experimental group. Each dot represents an individual animal. Representative cropped immunoblot bands are shown for each group (see Supplementary Fig. 5 and Source data Fig. 1). All data are expressed as mean ± s.e.m. Untreated $SOD1^{G37R}$ mice (**b**: $n = 4$), sham-operated $SOD1^{G37R}$ mice (**i**,**j**: $n = 12$; **t**,**u**,**v**: $n = 3$), AAV9–shRNA–*SOD1*-treated $SOD1^{G37R}$ mice (**b**: $n = 3$; **i**,**j**: $n = 9$; **t**,**u**,**v**: $n = 4$) and wild-type nontransgenic mice ($n = 3$). The statistical significance was determined using one-way ANOVA followed by Bonferroni's posthoc test (**b**, left graph: ANOVA $P < 0.0001$, $F = 46.65$; **b**, right graph: ANOVA $P = 0.0024$, $F = 16.16$; **i**: ANOVA $P = 0.0009$, $F = 10.06$; **j**: ANOVA $P < 0.0001$, $F = 23.60$; **t**, cervical: ANOVA $P < 0.0001$, $F = 57.14$; **t**, thoracic: ANOVA $P < 0.0001$, $F = 124.8$; **t**, lumbar: ANOVA $P < 0.0001$, $F = 692.1$; **u**, cervical: ANOVA $P = 0.0003$, $F = 33.663.60$; **u**, thoracic: ANOVA $P < 0.0001$, $F = 147.9$; **u**, lumbar: ANOVA $P < 0.0001$, $F = 48.15$; **v**: ANOVA $P < 0.0001$, $F = 93.37$). *P* values are shown between the indicated groups. DH, dorsal horn; VH, ventral horn.

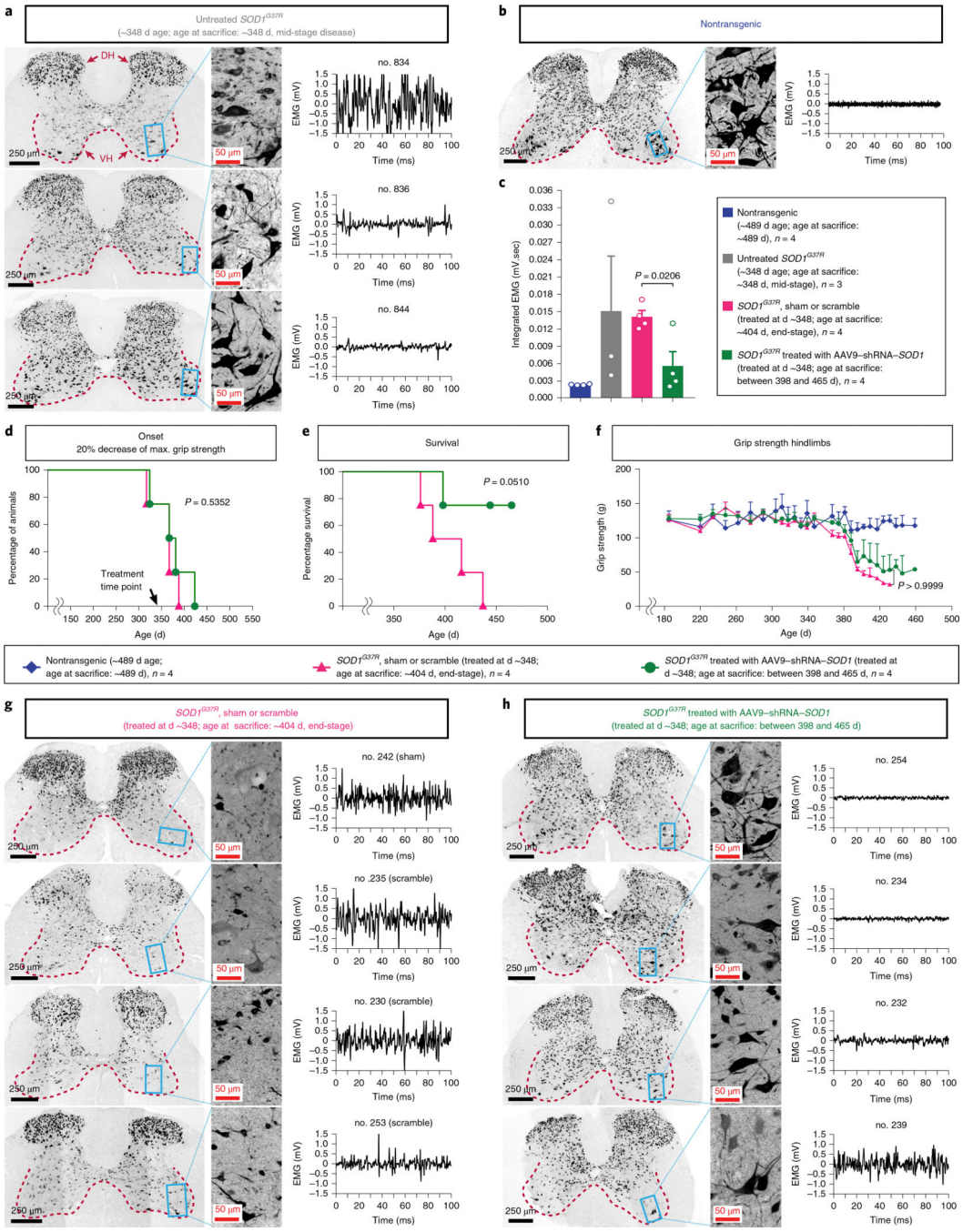

Fig. 5 |. Spinal SP AAV9–shRNA–*SOD1* delivery to symptomatic *SOD1*^{G37R} mice blocks further disease progression and preserves residual motor function.

a, Presence of fibrillations in the GCM and corresponding α-motoneuron degeneration in 348 ± 2-d-old *SOD1*^{G37R} mice. The result of three independent animals is shown. **b**, Baseline EMG activity (background) and normal spinal α-motoneuron morphology (visualized by immunofluorescence for NeuN) in wild-type nontransgenic age-matched (age 348 ± 2 d) mice. A representative result of four independent mice is shown. **c**, Quantitative analysis of MFs (integrated EMG signals) in all experimental groups. Each dot represents an

individual animal. **d**–**f**, Disease onset, survival (measured by loss of righting reflex) and hindlimb grip strength in nontransgenic *SOD1*^{G37R} and AAV9–shRNA–*SOD1*-treated *SOD1*^{G37R} mice. **g**, MF recording and corresponding lumbar spinal cord α-motoneuron degeneration (blue rectangle areas) in four individual sham-operated or scrambled virus-injected *SOD1*^{G37R} animals, recorded at the end-stage of disease. High-amplitude MFs and extensive α-motoneuron loss can be seen in all animals. **h**, MF recordings and corresponding lumbar spinal cord α-motoneuron preservation (rectangular areas) in four individual shRNA–*SOD1*-injected *SOD1*^{G37R} animals. Note the complete absence of MF with large α-motoneuronal protection in animals nos. 254 and 234. Data are expressed as mean ± s.e.m. Untreated *SOD1*^{G37R} mice (n = 3), sham or scramble and AAV9–shRNA–*SOD1*-treated *SOD1*^{G37R} mice (n = 4 for each group), AAV9–shRNA–*SOD1*-treated *SOD1*^{G37R} mice (n = 4) and wild-type nontransgenic mice (n = 4). All animals in **g** and **h** were sham/scramble-vector injected or treated with AAV9–shRNA–*SOD1* at age 348 ± 2 d. The statistical significance was determined as follows: **c**, unpaired, two-tailed, Student's t-test (d.f. = 6); **d**, Kaplan–Meier survival analysis using the two-sided log-rank test (there was no difference in median disease onset across *SOD1*^{G37R}, sham- or scramble-vector-treated *SOD1*^{G37R} mice (n = 4; 367 d) and AAV9–shRNA–*SOD1*-treated *SOD1*^{G37R} mice (n = 4, 374 d), with an average age at treatment of 348 d, P = 0.5352; **e**, Kaplan–Meier survival analysis using the log-rank test: median survival of AAV9–shRNA–*SOD1*-treated *SOD1*^{G37R} animals (n = 4, undefined; three of four animals continued to survive for a minimum of 451 d) versus *SOD1*^{G37R}, sham or scramble-operated mice (n = 4, 402 d; P = 0.0510); **f**, two-way ANOVA followed by Bonferroni's posthoc test (ANOVA $P_{int} < 0.0001$, F = 2.194). P values are shown between the indicated groups/time points.

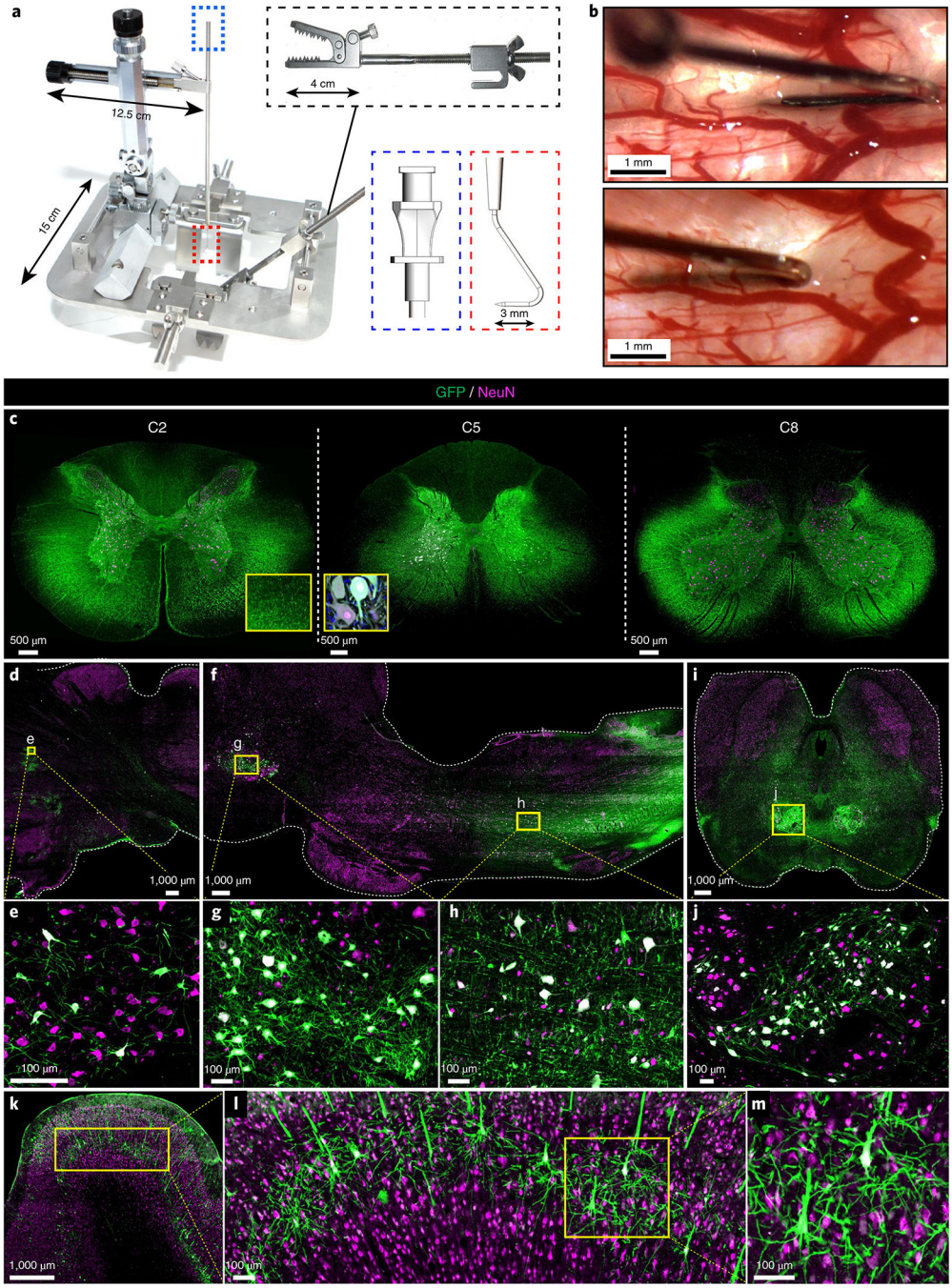

Fig. 6 |. Potent AAV9-mediated gene delivery into the cervical spinal cord and brain motor centers in adult pigs after a single-bolus SP AAV9–UBI–*GFP* injection.

a, Functional prototype of human SP injection device composed of a self-anchoring platform, built-in muscle retractors, spinal titanium clamps, *XYZ* manipulator (Narishige) and 27-G SP needle. The injector is used for SP vector delivery of AAV9–UBI–*GFP* (400 µl) into adult (35–45 kg) Gottingen–Minnesota pigs. **b**, SP injection needle just before and after placement into spinal cervical SP space. **c**, GFP expression in the white and gray matter of C2–C8 cervical segments (21 d after AAV9–UBI–*GFP* injection). **d**–**m**, Retrograde

transduction-induced GFP expression in tectal (**e**), rubral (**g**,**i**,**j**) reticular (**h**) and cortical–pyramidal (**k**–**m**) neurons. A representative result of three independent mini-pigs is shown.